

Journal Pre-proofs

Design, Synthesis, and biological evaluation of new series of pyrrol-2(3*H*)-one and pyridazin-3(2*H*)-one derivatives as tubulin polymerization inhibitors

Mahmoud S. Abdelbaset, Mostafa H. Abdelrahman, Syed Nasir Abbas Bukhari, Ahmed M. Gouda, Bahaa G. M. Youssif, Mohamed Abdel-Aziz, Gamal El-Din A. Abuo-Rahma

PII: S0045-2068(20)31820-4
DOI: <https://doi.org/10.1016/j.bioorg.2020.104522>
Reference: YBIOO 104522

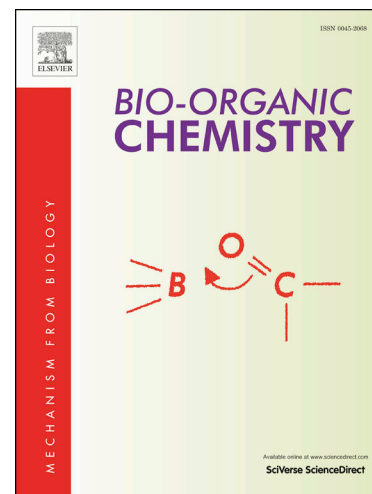
To appear in: *Bioorganic Chemistry*

Received Date: 2 September 2020
Revised Date: 21 October 2020
Accepted Date: 27 November 2020

Please cite this article as: M.S. Abdelbaset, M.H. Abdelrahman, S. Nasir Abbas Bukhari, A.M. Gouda, B. G. M. Youssif, M. Abdel-Aziz, G. El-Din A. Abuo-Rahma, Design, Synthesis, and biological evaluation of new series of pyrrol-2(3*H*)-one and pyridazin-3(2*H*)-one derivatives as tubulin polymerization inhibitors, *Bioorganic Chemistry* (2020), doi: <https://doi.org/10.1016/j.bioorg.2020.104522>

This is a PDF file of an article that has undergone enhancements after acceptance, such as the addition of a cover page and metadata, and formatting for readability, but it is not yet the definitive version of record. This version will undergo additional copyediting, typesetting and review before it is published in its final form, but we are providing this version to give early visibility of the article. Please note that, during the production process, errors may be discovered which could affect the content, and all legal disclaimers that apply to the journal pertain.

© 2020 Published by Elsevier Inc.



Design, Synthesis, and biological evaluation of new series of pyrrol-2(3H)-one and pyridazin-3(2H)-one derivatives as tubulin polymerization inhibitors

Mahmoud S. Abdelbaset ^a, Mostafa H. Abdelrahman ^a, Syed Nasir Abbas Bukhari ^b, Ahmed M. Gouda ^c, Bahaa G. M. Youssif ^d, Mohamed Abdel-Aziz ^e, Gamal El-Din A. Abuo-Rahma ^{e,f}

^a*Department of Pharmaceutical Organic Chemistry, Faculty of Pharmacy, Al-Azhar University, Assiut 71524, Egypt;* ^b*Department of Pharmaceutical Chemistry, College of Pharmacy, Jouf University, Aljouf, Sakaka 2014, Saudi Arabia;* ^c*Department of Medicinal Chemistry, Faculty of Pharmacy, Beni-Suef University, Beni-Suef 62514, Egypt;* ^d*Department of Pharmaceutical Organic Chemistry, Faculty of Pharmacy, Assiut University, Assiut 71526, Egypt;* ^e*Department of Medicinal Chemistry, Faculty of Pharmacy, Minia University, 61519-Minia, Egypt;* ^f *Department of Pharmaceutical Chemistry, Faculty of Pharmacy, Deraya University, New Minia, Minia, Egypt.*

Short running title: Synthesis and biological evaluation of new pyrrole and pyridazine derivatives

**To whom correspondence should be addressed:*

Gamal El-Din A. Abuo-Rahma, Ph.D. Department of Medicinal Chemistry, Faculty of Pharmacy, Minia University, 61519-Minia, Egypt.

Tel.:(002)-01003069431

E-mail address: gamal.aborahma@mu.du.eg

Bahaa G. M. Youssif, Ph.D. Pharmaceutical Organic Chemistry Department, Faculty of Pharmacy, Assiut University, Assiut 71526, Egypt.

Tel.: (002)-01098294419

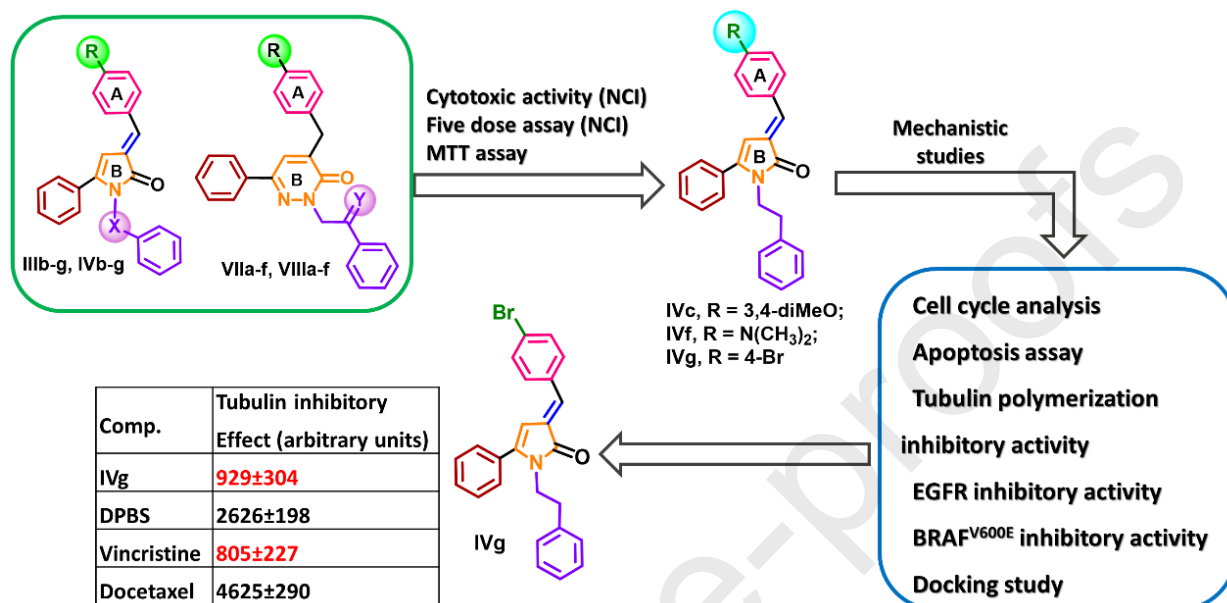
E-mail address: bahaa.youssif@pharm.aun.edu.eg, bgyoussif@ju.edu.sa

Abstract

A potential microtubule destabilizing series of new thirty-five Pyrrol-2-one, Pyridazin-3(2*H*)-one and Pyridazin-3(2*H*)-one/oxime derivatives has been synthesized and tested for their antiproliferative activity against a panel of 60 human cancer cell lines. Compounds **IVc**, **IVg** and **IVf** showed a broad spectrum of growth inhibitory activity against cancer cell lines representing renal, cancer of lung, colon, central nervous system, ovary, and kidney. Among them, compound **IVg** was found to have broad spectrum anti-tumor activity against the tested nine tumor subpanels with selectivity ratios ranging between 0.21 and 3.77 at the GI₅₀ level. *In vitro* assaying revealed tubulin polymerization inhibition by all active compounds **IVc**, **IVg** and **IVf**. The results of the docking study revealed nice fitting of compounds **IVc**, **IVf**, and **IVg** into CA-4 binding site in tubulin. The three compounds exhibited high binding affinities ($\Delta G_b = -12.49$ to -12.99 kcal/mol) toward tubulin compared to CA-4 (-8.87 kcal/mol). Investigation of the binding modes of the three compounds **IVc**, **IVf**, and **IVg** revealed that they interacted mainly hydrophobically with tubulin and similar binding orientations to that of CA-4. These observations suggest that tubulin is a possible target for these compounds.

Key words: Pyrrol-2-one, Pyridazin-3(2*H*)-one, Anti-proliferative, Tubulin and CA-4.

Graphical Abstract



Highlights

- A novel series of Pyrrol-2-one, Pyridazin-3(2*H*)-one derivatives has been synthesized and tested by NCI for their antiproliferative activity.
- The **IVc** and **IVg** compounds showed excellent activity and were further selected for a five-dose assay.
- *In vitro* antiproliferative activity of compounds **IVc**, **IVf**, and **IVg** was evaluated using MTT assay.
- Compounds **IVc**, **IVf**, and **IVg** have been evaluated against EGFR, BRAF^{V600E} and Tubulin anticancer targets.
- A docking study of compounds **IVc**, **IVf** and **IVg** showed a strong fitting to the CA-4 binding sites in tubulin.

1. INTRODUCTION

The main cytoskeletal filaments are microtubules composed by both α and β -tubulin proteins [1]. Microtubules play a significant role in many aspects of cellular processes, including cell division, shape maintenance, cell motility and vesicular transport [2-5]. The formation of microtubules has been shown to be a complex mechanism for the polymerization and the depolymerization of α/β heterodimers [6]. The disruption of this complex equilibrium impedes mitosis cell division, leading to metaphase cell cycle arrest and cell mortality [7]. Tubulin therefore became a promising target for the tumor therapy [8]. To date, several natural and synthetic tubulin-targeted compounds have been developed to treat malignancies. Most of these compounds have been classified into two major categories, one being the microtubule destabilizing agent that bind to vinblastine and the colchicine site, the other one is microtubule-stabilizing agents which bind to paclitaxel binding site and disturb tubulin disassembly [9-12]. Owing to the high toxicity to non-cancer cells, however, the FDA has not approved candidates that are bind to a colchicine site [13].

Pyridazinone and pyrrolone constitute interesting heterocyclic compounds with variable biological activities such as antibacterial [14,15], anti-inflammatory [16,17], vasodilators [18], antihypertensive [19] and anticancer activities [20-22]. Furthermore, some literature reports referred to the anticancer mechanism of pyridazinones and pyrrolones and provided an evidence that anticancer mechanism of pyridazinones through tubulin polymerization inhibition [23]. Both pyridazinones and pyrrolones could be synthesized by nucleophilic substitution from the corresponding furanones [24]. Pyridazinones and pyrrolones are perfectly clinically appropriate moieties. The most important examples are, Althiomycin **1** [25] which is a naturally occurring

alkaloid separated from *Streptomyces Althioticus* and used as antibiotic through inhibition of protein synthesis. In addition, Pimobendan (**2**) [26] is a phosphodiesterase III (PDEIII) inhibitor and used in management of congestive heart failure. Moreover, Emorfozan (**3**) [27] was marketed in Japan as an analgesic and anti-inflammatory drug, **Fig. 1**.

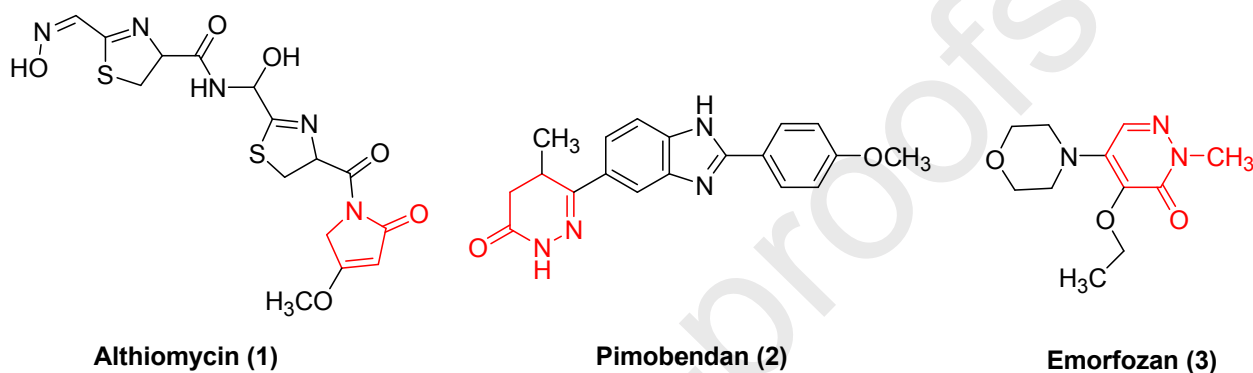


Fig. 1. Structure of pyridazinone and pyrrolone -based clinically used drugs

Accordingly, based on the above data on the biological relevance of both pyridazinone and pyrrolone [21, 22], we report herein the design and synthesis of novel two series of pyridazinone and pyrrolone (**Scaffolds A and B, Fig. 2**) as promising anticancer candidates. The target compounds were tested for antiproliferative action. In addition, a mechanistic study of BRAF^{V6000}, EGFR Tk kinases and tubulin polymerization inhibitor activity were evaluated. In addition, cell cycle analysis and apoptosis assay have been established for the most active compound.

1.1. Rational design of the new compounds

Previously, we have reported compound **4e** (Fig. 2) as CA-4 analog with potent cytotoxic activity ($IC_{50} = 1.9-4.9 \mu M$) among a series of pyrrol-2(3*H*)-one derivatives [22]. Mechanistic study of compound **4e** revealed potent tubulin polymerization inhibitory activity. In attempt to optimize the anticancer potential of **4e** in the current study, we have performed a series of structural modifications aiming to improve the binding affinity to tubulin protein. The structural modifications in compound **4e** included combining both alkylation of the pyrrole NH group with aralkyl(benzyl/phenethyl) and replacement of the 2-(methylthio) quinoline by aryl ring. The result of these improvements is the ability to build extra-binding hydrophobic pockets that can contribute to improving binding affinity for tubulin protein, as assessed in a preliminary docking study. The results of this study revealed improvement in binding affinities of the *N*-phenethyl derivatives ($\Delta G_b = 12.60-12.99$ kcal/mol) compared to 11.82 kcal/mol for compound **4e**.

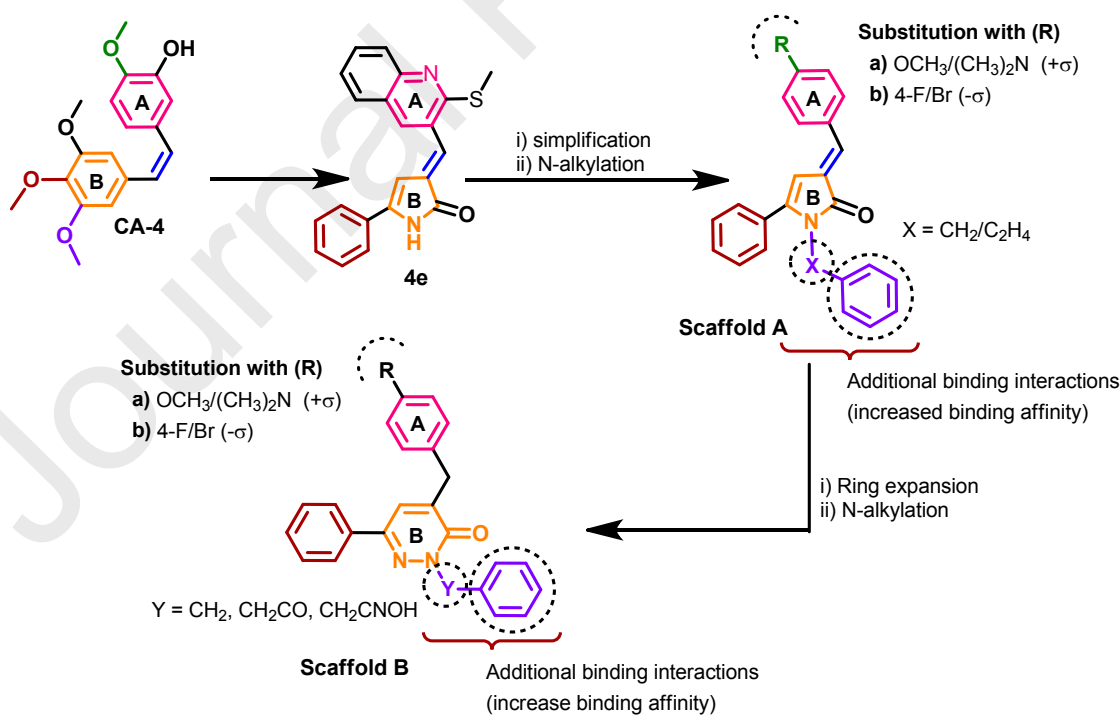


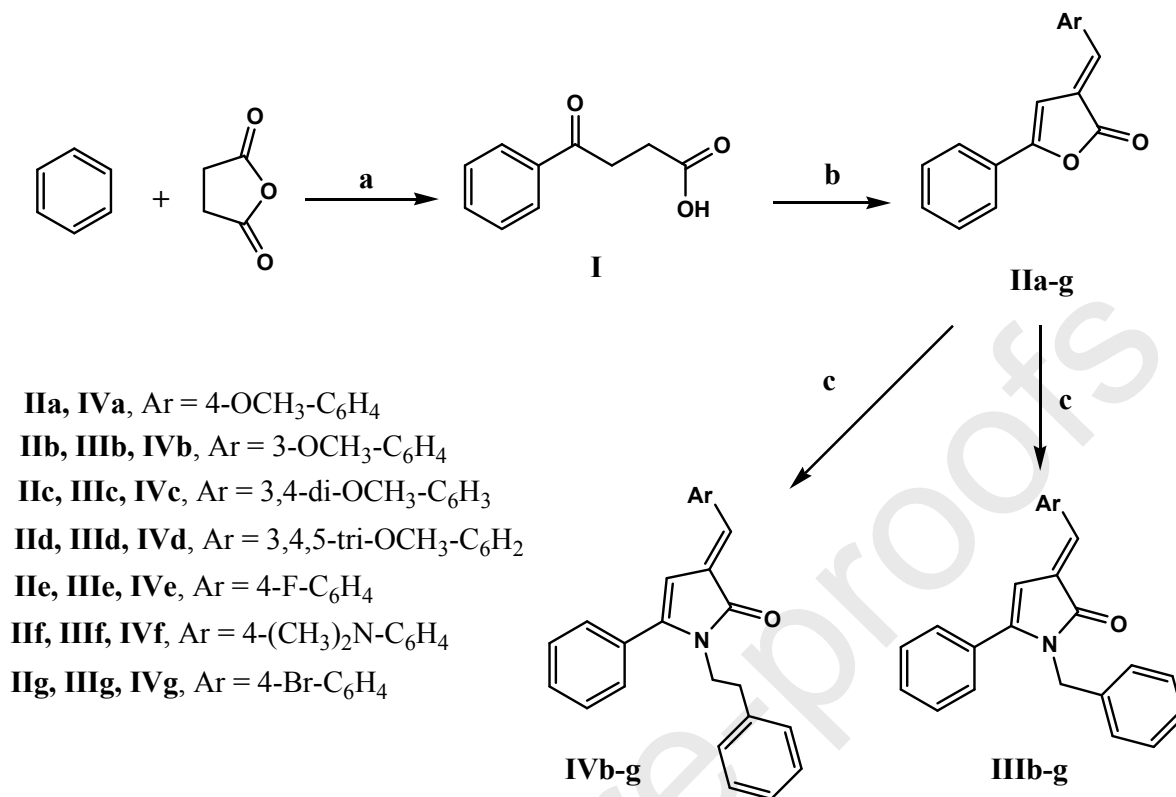
Fig. 2. Rational design and structural modifications of **scaffolds A and B**

The study of SAR of **scaffold A** also included substitution on ring A in **scaffold A** was done using the electron-donating mono/di/tri-methoxy groups to mimic ring A in CA-4. In addition, electron-withdrawing groups (4-F/Br) were also used to evaluate the impact of electronic effect of different substituents on activity of the new compounds. Furthermore, **scaffold B** was designed by expansion of the pyrrole ring into pyridazin-3(2*H*)-one ring with *N*-alkylation. **Scaffold B** was also functionalized with hydrogen bond donor/acceptor groups to investigate the impact of these groups on activity and binding affinities to tubulin protein.

2. RESULTS AND DISCUSSION

2.1. Chemistry

The synthesis of *N*-benzyl and *N*-phenethyl-1*H*-pyrrol-2(3*H*)-ones **IIIb-g** and **IVa-g** was shown in **Scheme 1**. The reflux of benzene and succinic anhydride in hood under the Friedl Craft acylation produced 3-Benzoyl-propionic acid **I** with good yield [28]. Perkin condensation of **I** in the presence of triethylamine (TEA) and drops of acetic anhydride with various aromatic aldehydes gave corresponding furanones **IIa-g** [29].



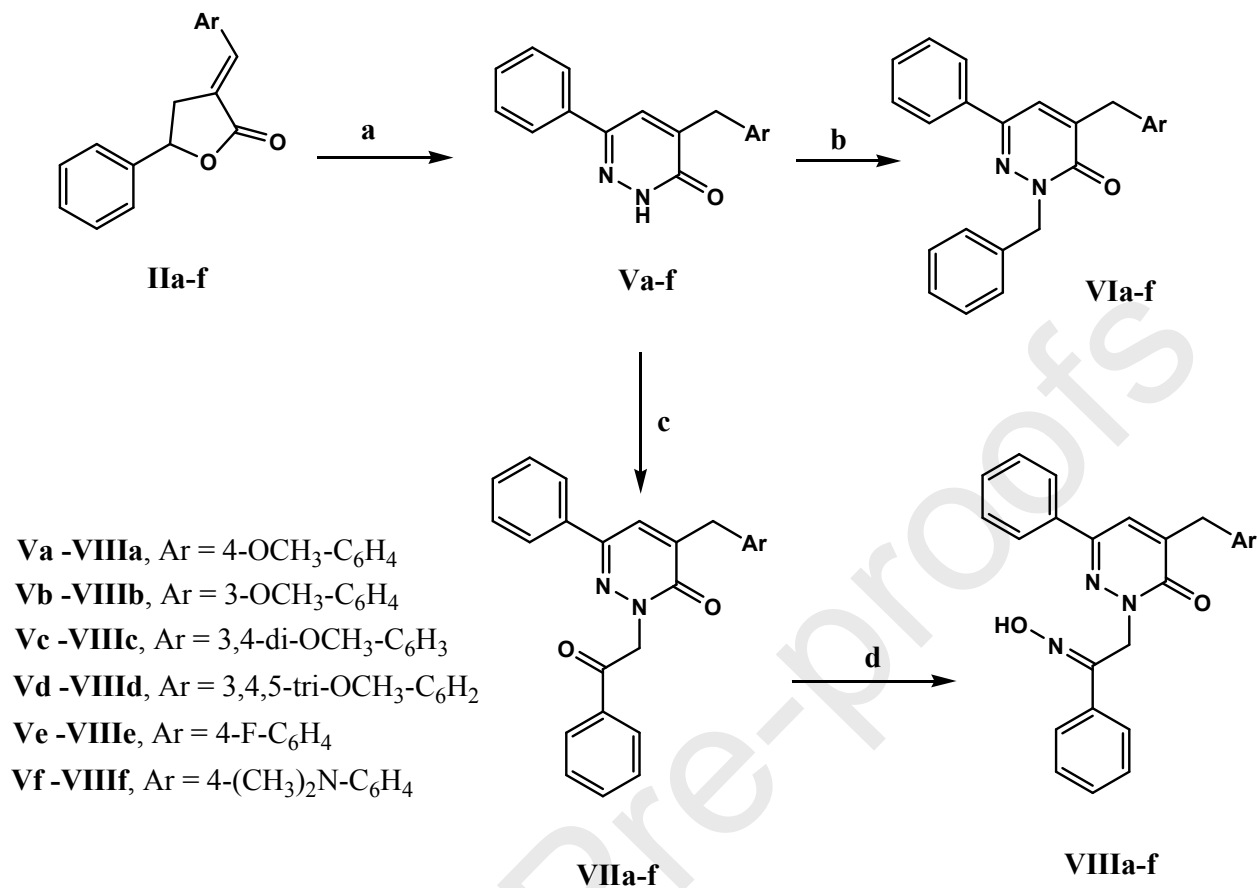
Scheme 1. Synthesis of *N*-benzyl and *N*-phenethyl-1*H*-pyrrol-2(3*H*)-ones **IIIb-g** and **IVa-g**

Reagent and reaction conditions: a) Anhydrous AlCl₃, reflux, 30 mins; b) Ar-CHO, (CH₃CO)₂O, TEA, fusion, 15 mins; c) Benzylamine or phenethylamine, EtOH, reflux, 3h.

The corresponding pyrrol-2-(3*H*)-ones **IIIb-g** and **IVa-g** were given respectively by heating furanones **IIa-g** with benzylamine or phenethylamine in ethanol. The structure of **IIIb-g** and **IVa-g** was confirmed by IR, NMR and HRESI-MS spectroscopy. ¹H NMR spectra of compounds **IIIb-g** showed a common peak appeared as doublet of doublet at δ 4.08-4.14 to 4.33-4.36 ppm with coupling constant (*J* = 15.3 Hz) associated with the geminal coupling of the diastereotopic benzylic protons, which may be due to the effect of configuration around the exocyclic double bond in C-3. The ¹³C NMR spectra of the pyrrolone derivatives **IIIb-g** showed the characteristic benzylic carbons at δ 43.4 and 44.4 ppm and the (C=O) at 168.0 ppm. The olefinic and aromatic carbons appeared at their expected chemical shifts. Similarly, the ¹H NMR

spectra of compounds **IVa-g** showed four common signals appeared as doublet of doublet of doublet at δ 3.49-2.55 ppm related to (CH₂CH₂) of phenethyl group with coupling constant 13.4, 11.5, 5.2 Hz. The ¹³C NMR spectra of **IVa-g** showed the characteristic two signals at δ 44.1 ppm related to (N-CH₂) and 34.6 ppm related to the benzylic protons. Another significant signal appeared at 168.0 ppm related to the (C=O) group. The olefinic and aromatic carbons appeared at their expected chemical shifts. The purity of the prepared compounds was confirmed by HRESI-MS spectroscopy and the results are in consistent with the molecular formula of the products.

The synthesis of target derivatives **VIa-f**, **VIIa-f** and **VIIIa-f** was illustrated in **Scheme 2**. The 4,6-disubstituted pyridazin-3(2*H*)-ones **Va-f** were prepared by heating furanone derivatives **IIa-f** with hydrazine hydrate in absolute ethanol [30]. The IR spectra of pyridazinones **Va-f** showed medium stretching band at 3500-3269 cm⁻¹ related to (CONH) and strong stretching band at 1676-1652 cm⁻¹ related to (C=O), which are consistent with the proposed structure.



Scheme 2. Synthesis of pyridazinones and oximes

Reagent and reaction conditions: a) NH₂NH₂.H₂O, EtOH, reflux, 12h; b) Benzyl bromide, NaOEt, r.t, 12h.; c) Phenacyl bromide, NaOEt, r.t, 12 h.; d) NH₂OH, anhydrous sodium sulphate, EtOH, reflux, 6 h.

In the ¹H NMR of compounds **Va-f**, two common singlet signals one at 13.10-13.18 ppm related to pyridazinone ring (NHCO) and the other at 3.73-3.86 ppm associated with the benzylic protons. The ¹³C NMR spectra of **Va-f** showed the characteristic benzylic carbon at 35.1 ppm and the (C=O) at 168 ppm. The olefinic and aromatic carbons appeared at their expected chemical shifts. Stirring of pyridazin-3(2*H*)-ones **Va-f** with equimolar amount of benzyl or phenethyl bromides at room temperature in sodium ethoxide, afforded the corresponding *N*-benzylated pyridazin-3-ones **VIa-f** and *N*-phenethyl pyridazine-3-ones **VIIa-f**, respectively. It is

worth to note that carrying out the alkylation reaction in acetone/ K_2CO_3 for 24 h at room temperature gave no product; the same results were obtained upon heating in DMF using K_2CO_3 as a base. Also, no product was formed upon using TEA as a base and acetonitrile as a solvent on cold or reflux conditions. On the other hand, the use of NaOH and DMF gave a very low yield, difficult to be purified. So, the presence of strong base like sodium ethoxide is important for this type of alkylation reaction [28]. The IR spectra of compounds **VIa-f** showed strong stretching bands at 1655-1648 cm^{-1} related to (C=O) and 1632-1601 cm^{-1} related to (C=C), which are in consistent with the proposed structures. In the 1H NMR spectra of compounds **VIa-f** two common singlet signals one at 3.77-3.89 ppm related to (CH_2 benzylic) attached to the 4 position on the pyridazinone ring and the second at 5.33-5.36 ppm related to (N-benzylic CH_2). The IR spectra of compounds **VIIa-f** showed strong stretching bands at 1706-1696 cm^{-1} related to ($CH_2C=O$) and 1659-1632 cm^{-1} related to (N $C=O$), which are consistent with the proposed structures. In the 1H NMR spectra of compounds **VIIa-f** two singlet signals were common; one at 5.74-5.78 ppm related to (N CH_2CO) on the 2 position of pyridazinone ring and the second at 3.75-3.91 ppm related to (4-benzylic CH_2) protons. Finally, heating *N*-alkylated pyridazinones **VIIa-f** with hydroxylamine hydrochloride in absolute ethanol in presence of anhydrous sodium sulfate as a dehydrating agent afforded the corresponding oximes **VIIIa-f**. The IR spectra of oximes **VIIIa-f** showed significant stretching bands at 3327-3219 cm^{-1} related to (OH), 1647-1636 cm^{-1} related to (N $C=O$) and absence of stretching band at 1706-1689 cm^{-1} related to ($CH_2C=O$) characteristic of respective ketones **VIIa-f** which are in consistent with the proposed structures. In the 1H NMR spectra of **VIIIa-f** a common singlet signals were observed at 11.64-11.67 ppm related to (=N-OH), at 3.73-3.85 ppm associated with benzylic protons and at 5.46-5.50 of (N CH_2CO). Moreover, the 1H NMR results showed that oxime exist as two

diastereomers major in 82-88 % and minor in 12-18 %. These results are in agreement with a literature results that refer to the presence of oxime in the two diastereomeric forms syn and anti as illustrated [29]. The purity of the prepared compounds was confirmed by HRESI-MS spectroscopy and the results are in consistent with the molecular formula of the products.

2.2. Evaluation of biological Activities

2.2.1. Screening of cytotoxic activity

For screening of the target compounds to detect their potential antiproliferative activity against a panel of 60 cancer cell lines; compounds **IIIb-d**, **IVa-g**, **VIb-f**, **VIIa-e** and **VIIIa-f** were selected for screening according to NCI-guidelines at concentration of 10 μ M. The results for each compound (**Table 1**) were reported as the percent of growth inhibition of treated cells compared to untreated control cells. Generally, for **Scaffold A**, compounds **IVa-g** possessing *N*-phenethyl-1*H*-pyrrol-2(3*H*)-one were more active than **IIIb-d** possessing *N*-benzyl-1*H*-pyrrol-2(3*H*)-one which directly reflects the influences of *N*-phenethyl moiety on the antiproliferative activity of the title scaffold. Compounds **IVc** and **IVg** possessing 3,4-di-OCH₃ and 4-Br substituent showed a complete cell death against non-small cell lung cancer cell line HOP-62, CNS cancer cell line SNB-75 and ovarian cancer cell line OVACAR-4 with growth inhibition percentage of -29.96, -7.78 and -5.49 for compound **IVc**, (**Table 1**) and -56.85, -34.27 and -17.07 for compound **IVg**, respectively. Also, compound **IVc** exhibited a complete cell death against leukemia cancer cell line SR, non-small cell lung cancer cell line HOP-92, ovarian cancer cell line SK-OV-3 and renal cancer cell line A498, ACHN, RXF 393, TK-10 and UO-31 with growth inhibition percentage of -1.98, -4.05, -30.33, -75.37, -32.49, -3.29, -3.91 and -47.49, respectively (**Table 1**). Furthermore, compound **IVg**, showed a complete cell death against non-small cell lung cancer cell line HOP-92 and NCI-H226, CNS cancer cell line SF-295 and renal cancer cell line 786-0 with growth

percentage of -13.88, -1.06, -25.59 and -8.73, respectively (**Table 1**). In addition, the two compounds recorded significant activity against non-small cell lung cancer cell line NCI-H460, ovarian cancer cell line OVCAR-8 and breast cancer cell line HS 578T with growth inhibition percentage 20.50, 25.86 and 13.10 for compound **IVc** and 25.57, 17.68 and 22.81 for compound **IVg**, respectively. Moreover, compound **IVf** [(Ar = 4-(CH₃)₂N-C₆H₄)] showed a complete cell death against non-small cell lung cancer cell line HOP-62, CNS cancer cell line SNB-75, and ovarian cancer cell line OVCAR-4 with growth inhibition percentage -13.97, -29.13 and -11.62.

On the other hand, compounds **VIb-f**, **VIIa-e**, and **VIIIa-f** (**scaffold B**) showed moderate activity against the cancer cell lines studied. Compounds **VIc** and **VIId** possessing *N*-benzylated pyridazin-3-one moiety showed good activities against most of cancer cell lines with growth inhibition percentage between 6 to 26, **Table 1**. Compound **VIc** exhibited a complete cell death against leukemia cancer cell line SK-MEL-5 and renal cancer cell line A498 with growth inhibition rate of -3.54 and -16.92, see supplementary data.

Table 1. One dose assay of nine different cancer cell types of compounds **IVc**, **IVg**, **VIc**, **VId**, **VIIIe** and **VIIIf**.

Subpanel cancer cell Lines	Growth% inhibition						
	IVc	IVg	VIc	VId	VIIIe	VIIIf	
Leukemia							
CCRF-CEM	57.58	100.75	43.01	34.84	34.61	46.58	
HL-60(TB)	<u>19.64</u>	83.78	<u>25.79</u>	<u>19.26</u>	<u>24.81</u>	54.26	
K-562	47.56	75.54	<u>22.19</u>	<u>20.61</u>	<u>29.16</u>	<u>29.51</u>	
SR	<u>-1.98</u>	58.56	40.16	36.03	<u>30.27</u>	46.26	
MOLT4	ND	ND	<u>9.10</u>	<u>5.01</u>	<u>16.10</u>	35.11	
RPMI-8226	70.57	101.47	<u>15.20</u>	<u>24.84</u>	<u>25.63</u>	<u>28.24</u>	
Non-Small Cell Lung Cancer							
A549/ATCC	32.86	<u>8.19</u>	<u>20.00</u>	<u>19.88</u>	<u>24.22</u>	<u>30.24</u>	
EKVX	56.08	40.11	<u>14.44</u>	<u>14.65</u>	<u>29.13</u>	49.54	
HOP-62	<u>-29.96</u>	<u>-56.85</u>	90.91	66.12	62.69	75.05	
HOP-92	<u>-4.05</u>	<u>-13.88</u>	<u>28.04</u>	51.08	42.59	55.86	
NCI-H226	<u>29.71</u>	<u>-1.06</u>	51.28	46.20	57.08	60.47	
Colon Cancer							
COLO 205	Nd	<u>30.35</u>	113.74	102.03	47.91	58.45	
HCT-116	32.78	<u>22.73</u>	96.80	65.92	35.09	45.96	
HT-29	38.65	<u>32.5</u>	<u>10.55</u>	81.50	<u>20.25</u>	32.93	
CNS Cancer							
SF-295	<u>26.78</u>	<u>-25.59</u>	<u>28.78</u>	31.45	52.64	65.78	
SNB-75	<u>-7.78</u>	<u>-34.27</u>	58.12	94.45	72.92	57.77	
U251	<u>15.88</u>	<u>6.97</u>	65.14	87.54	44.31	34.54	
Melanoma							
LOX IMVI	<u>2.28</u>	42.19	48.44	43.65	53.09	53.03	
MALME-3M	39.30	50.52	<u>23.43</u>	35.16	35.81	66.17	
SK-MEL-5	38.47	70.06	<u>-3.54</u>	40.17	36.64	55.83	
UACC-62	54.48	46.59	<u>30.62</u>	37.69	33.59	39.26	
Ovarian Cancer							

OVCAR-3	<u>27.98</u>	42.10	47.52	46.94	94.88	56.16
OVCAR-4	<u>-5.49</u>	<u>-17.07</u>	<u>32.5</u>	35.29	85.47	55.05
OVCAR-8	<u>25.86</u>	<u>17.68</u>	<u>32.32</u>	<u>31.95</u>	88.75	57.21
NCI/ADR-RES	31.63	<u>27.79</u>	<u>30.16</u>	<u>30.50</u>	82.78	44.12
SK-OV-3	<u>-30.33</u>	<u>15.36</u>	74.06	82.27	104.97	94.61

Renal Cancer

786-0	<u>8.93</u>	<u>-8.73</u>	35.84	<u>49.93</u>	<u>69.22</u>	75.37
A498	<u>-75.37</u>	50.83	<u>-16.92</u>	51.14	<u>9.60</u>	<u>-3.20</u>
ACHN	<u>-32.49</u>	<u>13.00</u>	<u>27.12</u>	<u>27.90</u>	40.26	52.75
RXF 393	<u>-3.29</u>	31.53	42.38	<u>31.68</u>	<u>28.51</u>	61.40
TK-10	<u>-3.91</u>	<u>12.62</u>	49.81	45.21	63.49	84.52
UO-31	<u>-47.49</u>	45.00	<u>14.71</u>	<u>21.57</u>	<u>30.93</u>	36.13

Breast Cancer

MCF7	<u>29.63</u>	<u>24.79</u>	<u>19.94</u>	<u>24.52</u>	<u>26.22</u>	<u>29.08</u>
MDA-MB-231/ATC	ND	ND	43.65	50.06	43.08	53.95
HS 578T	<u>13.10</u>	<u>22.81</u>	66.62	74.90	73.84	<u>83.09</u>
T-47D	<u>8.00</u>	50.52	<u>7.51</u>	<u>6.19</u>	<u>11.83</u>	<u>11.78</u>

2.2.2 *In vitro* five dose full NCI 60 cell panel assay

Compound **IVc** and **IVg** were selected for advanced five dose testing, where the cytotoxic and/or growth inhibitory effects of the tested compound was tested *invitro* against the full panel of 60 human tumor cell lines derived from nine neoplastic diseases at 10 fold dilutions of five concentrations ranging from 10^{-4} M to 10^{-8} M. Three dose response parameter were calculated for each cell line, GI_{50} (Growth inhibitory activity) corresponds to concentration of the compound causing 50% inhibition of net cell growth, TGI value (cytostatic activity) corresponds to the concentration of the compound resulting in total growth inhibition and LC_{50} value (cytotoxic activity) is the concentration of the compound causing net 50% loss of initial cells at the end of incubation period of 48 h. Additionally, (MG_MID) is calculated for each mentioned parameter, which displays an averaged activity parameter over all cell lines, as well as the delta parameter and the range were also calculated. The $\log_{10} GI_{50}$, $\log_{10} TGI$, $\log_{10} LC_{50}$ were then determined, defined as the means of the $\log_{10, s}$ of the individual GI_{50} , TGI, LC_{50} value. Negative values indicated the most sensitive cell lines. Compound having $\log_{10} GI_{50}$ values -4 and < -4 is declared to be active. The results of the NCI-60 5-dose assay are shown in **Tables 2 and 3, Fig. 3 and 4**. **IVc** and **IVg** displayed strong antiproliferative properties. The best candidate for growth inhibition properties was compound **IVg**, with GI_{50} values $< 1 \mu\text{M}$ against 13 cell lines, particularly for non-small cell lung cancer HOP 62 ($GI_{50} = 0.35 \mu\text{M}$) and HOP 92 ($GI_{50} = 0.32 \mu\text{M}$) cells, CNS SF-295 cells ($GI_{50} = 0.33 \mu\text{M}$), renal cancer 786-0, A498, and ACHN cells ($GI_{50} = 0.65 \mu\text{M}$) and breast cancer HS578T cells ($GI_{50} = 0.83 \mu\text{M}$). Compound **IVg** showed good antiproliferative activity against all melanoma cancer, ovarian cancer, and prostate cell lines with GI_{50} ranging from 0.82 to 8.38 μM .

Compound **IVc** showed considerable antiproliferative activity against all CNS cancer, ovarian cancer, and ovarian cell lines with GI_{50} ranging from 1.89 to 9.03 μM . but also on some cell lines from non-small cell lung cancer, colon cancer, and breast cancer, respectively.

Evaluation of selectivity of a compound depends upon the ratio obtained by dividing the full panel MID^a (the average sensitivity of all cell lines toward the test agent μM) by their individual subpanel MID^b (μM). Ratios between 3 and 6 refer to moderate selectivity; ratios > 6 indicate high selectivity toward the corresponding cell line, while compounds not meeting either of these criteria rated non-selective. Compound **IVc** was found to have broad-spectrum antitumor activity against the nine tumor subpanels tested with selectivity ratios ranging from 0.43 to 2.26 at the GI_{50} level, **Table 2**, and **Fig. 3**. While compound **IVg** was found to have broad-spectrum antitumor activity against the nine tumor subpanels examined, with selectivity ratios ranging from 0.21 to 3.77 at GI_{50} level. **IVg** exhibited moderate selectivity toward the CNS cancer and renal cancer subpanels with selectivity ratio of 3.77 and 3.13 respectively, at GI_{50} level. See **Table 3**, **Fig. 4**, and supplementary data.

Table 2. Selectivity of compound **IVc** on sixty human cancer types

Panel	Cell line	GI ₅₀ (μM)			TGI	LC ₅₀
		Conc.per cell line	Subpanel MID ^b	Selectivity ratio		
Leukemia	CCRF-CEM	35.90	20.2	0.43	>100	>100
	HL-60(TB)	11.70			68.6	>100
	K-562	23.90			>100	>100
	RPMI-8226	18.4			84.9	>100
	SR	11.10			57.7	>100
Non-small cell lung cancer	A549/ATCC	5.06	7.58	1.14	17.7	54.7
	EKVX	10.40			54.0	>100
	HOP-62	2.72			10.0	>100
	HOP-92	2.54			8.17	57.5
	NCI-H226	4.60			30.2	>100
	NCI-H23	17.00			>100	>100
	NCI-H322M	8.77			33.2	>100
	NCI-H460	7.34			30.7	>100
	NCI-H522	9.80			36.0	>100
Colon cancer	COLO 205	17.30	12.73	0.68	>100	>100
	HCC-2998	12.90			64.1	>100
	HCT-116	3.09			11.6	34.0
	HCT-15	11.10			>100	>100
	HT29	8.92			48.9	>100
	KM12	22.20			>100	>100
	SW-620	13.6			>100	>100
CNS cancer	SF-268	8.18	5.16	1.67	26.0	76.5
	SF-295	5.95			24.0	70.4
	SF-539	6.68			23.5	63.4
	SNB-19	5.08			21.0	71.4
	SNB-75	1.89			6.28	45.7
	U251	3.20			9.31	32.3
Melanoma	LOX IMVI	5.94	10.06	0.86	19.0	45.1
	MALME-3M	10.20			61.9	>100
	M14	8.84			>100	>100
	MDA-MB-435	4.78			>100	>100
	SK-MEL-2	18.5			>100	>100
	SK-MEL-28	6.76			68.1	>100
	SK-MEL-5	9.29			94.5	>100
	UACC-257	20.20			86.8	>100
	UACC-62	6.01			40.9	>100
Ovarian Cancer	IGROV1	4.93	5.49	1.57	52.1	>100
	OVCAR-3	4.82			17.8	48.5
	OVCAR-4	3.15			87.0	>100
	OVCAR-5	6.37			73.1	>100
	OVCAR-8	6.09			22.5	72.9
	NCI/ADR-RES	9.03			68.5	>100

	SK-OV-3	4.04			18.8	94.6
Renal Cancer	786-0	2.14	3.83	2.26	5.85	20.8
	A498	2.25			5.32	42.0
	ACHN	3.53			14.0	48.3
	CAKI-1	7.53			>100	>100
	RXF 393	3.64			15.6	42.0
	SN12C	4.88			21.8	85.4
	TK-10	2.28			4.91	16.0
	UO-31	4.35			20.6	63.1
Prostate Cancer	PC-3	21.1	17.15	0.50	>100	>100
	DU-145	13.2			>100	>100
Breast Cancer	MCF7	4.18	5.86	1.47	57.2	>100
	MDA-MB-231/ATCC	4.16			17.9	65.6
	HS 578T	3.66			23.4	>100
	BT-549	12.40			29.9	>100
	T-47D	3.20			48.1	>100
	MDA-MB-468	7.57			42.4	>100
MID^a			8.64			

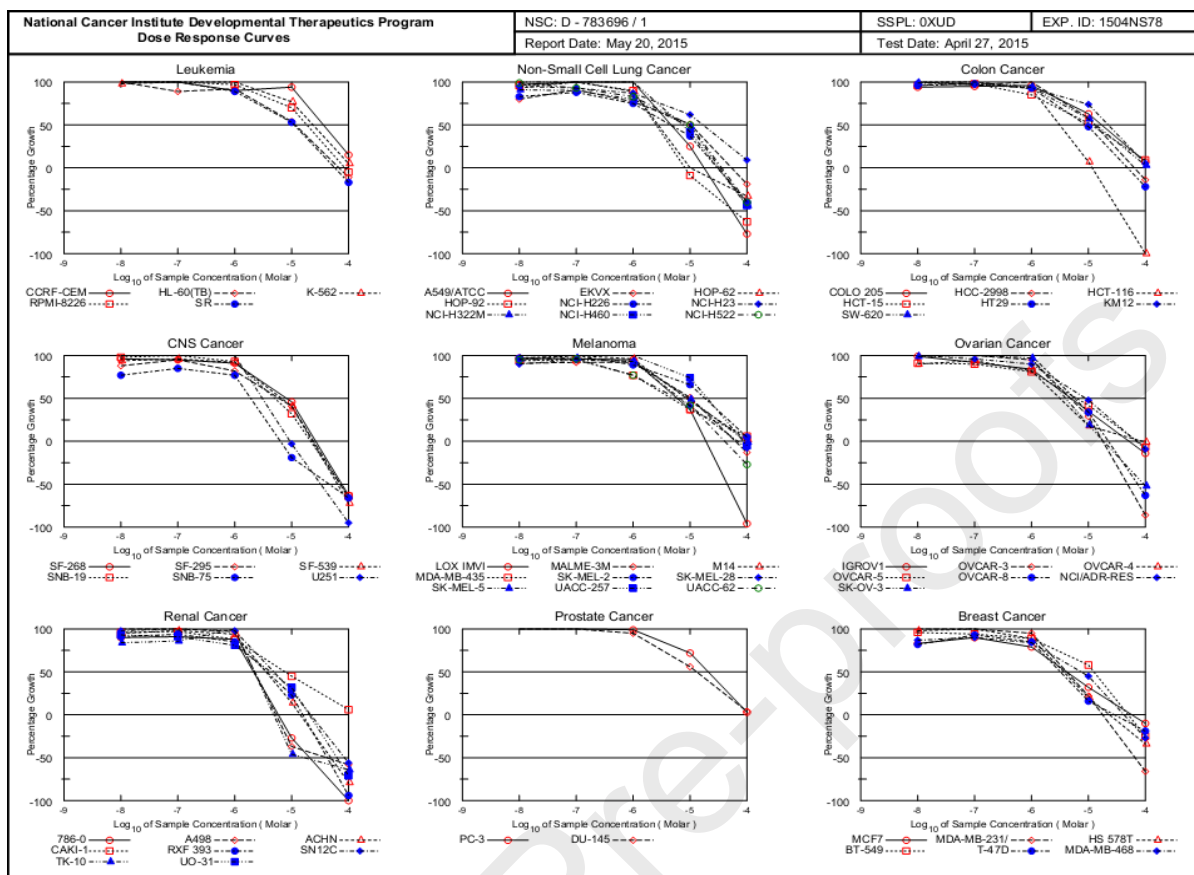


Fig. 3. Concentration-antiproliferative response curves of compound **IVc** against sixty different cancer cell lines

Table 3. Selectivity of compound **IVg** on sixty human cancer types.

Panel	Cell line	GI ₅₀ (μM)			TGI	LC ₅₀
		Conc.per cell line		Subpanel MID ^b		
		Conc.per cell line	Selectivity ratio			
Leukemia	CCRF-CEM	7.76	20.82	0.21	>100	>100
	HL-60(TB)	75.10			>100	>100
	K-562	2.63			20.5	>100
	MOLT-4	18.40			>100	>100
	RPMI-8226	9.44			86.4	>100
	SR	11.60			>100	>100
Non-small cell lung cancer	A549/ATCC	1.37	1.72	2.54	11.9	57.4
	EKVX	1.95			19.0	95.6
	HOP-62	0.35			1.22	4.51
	HOP-92	0.32			2.63	18.3
	NCI-H226	1.11			4.57	56.7
	NCI-H23	1.69			14.6	67.5
	NCI-H322M	1.20			18.8	>100
	NCI-H460	0.91			10.2	46.1
	NCI-H522	6.54			87.1	>100
Colon cancer	COLO 205	3.26	5.12	0.82	27.6	>100
	HCC-2998	7.52			>100	>100
	HCT-116	0.39			11.7	57.6
	HCT-15	11.70			>100	>100
	HT29	4.73			>100	>100
	KM12	43.60			>100	>100
	SW-620	5.34			>100	>100
CNS cancer	SF-268	2.27	1.16	3.77	16.3	>100
	SF-295	0.33			1.59	6.23
	SF-539	1.77			5.57	24.0
	SNB-19	1.21			5.03	47.5
	SNB-75	0.66			3.83	31.3
	U251	0.76			10.1	43.3
Melanoma	LOX IMVI	0.82	3.52	1.24	10.8	36.9
	MALME-3M	1.50			6.64	42.5
	M14	3.53			71.8	>100
	MDA-MB-435	8.38			>100	>100
	SK-MEL-2	4.47			27.2	>100
	SK-MEL-28	2.75			17.0	>100
	SK-MEL-5	3.89			20.8	87.3
	UACC-257	2.82			18.7	>100
Ovarian Cancer	IGROV1	1.71	1.71	2.56	12.0	61.9
	OVCAR-3	1.78			7.34	35.0
	OVCAR-4	0.55			3.13	19.6
	OVCAR-5	4.28			40.2	>100
	OVCAR-8	1.04			10.0	48.0
	NCI/ADR-RES	1.08			8.02	53.9

	SK-OV-3	1.55			5.00	26.0
Renal Cancer	786-0	0.65	1.14	3.13	2.80	10.5
	A498	0.65			5.44	69.6
	ACHN	0.65			11.0	65.8
	CAKI-1	1.23			7.60	40.7
	RXF 393	1.26			3.78	13.7
	SN12C	2.15			20.4	>100
	TK-10	1.82			6.06	35.6
	UO-31	2.82			19.8	>100
Prostate Cancer	PC-3	1.20	1.87	2.34	5.06	27.4
	DU-145	2.54			15.8	82.3
Breast Cancer	MCF7	3.42	3.85	1.14	32.7	>100
	MDA-MB-231/ATCC	1.67			24.7	>100
	HS 578T	0.83			5.34	>100
	BT-549	2.59			9.06	47.2
	T-47D	13.30			>100	>100
	MDA-MB-468	1.27			7.80	>100
MID^a			4.38			

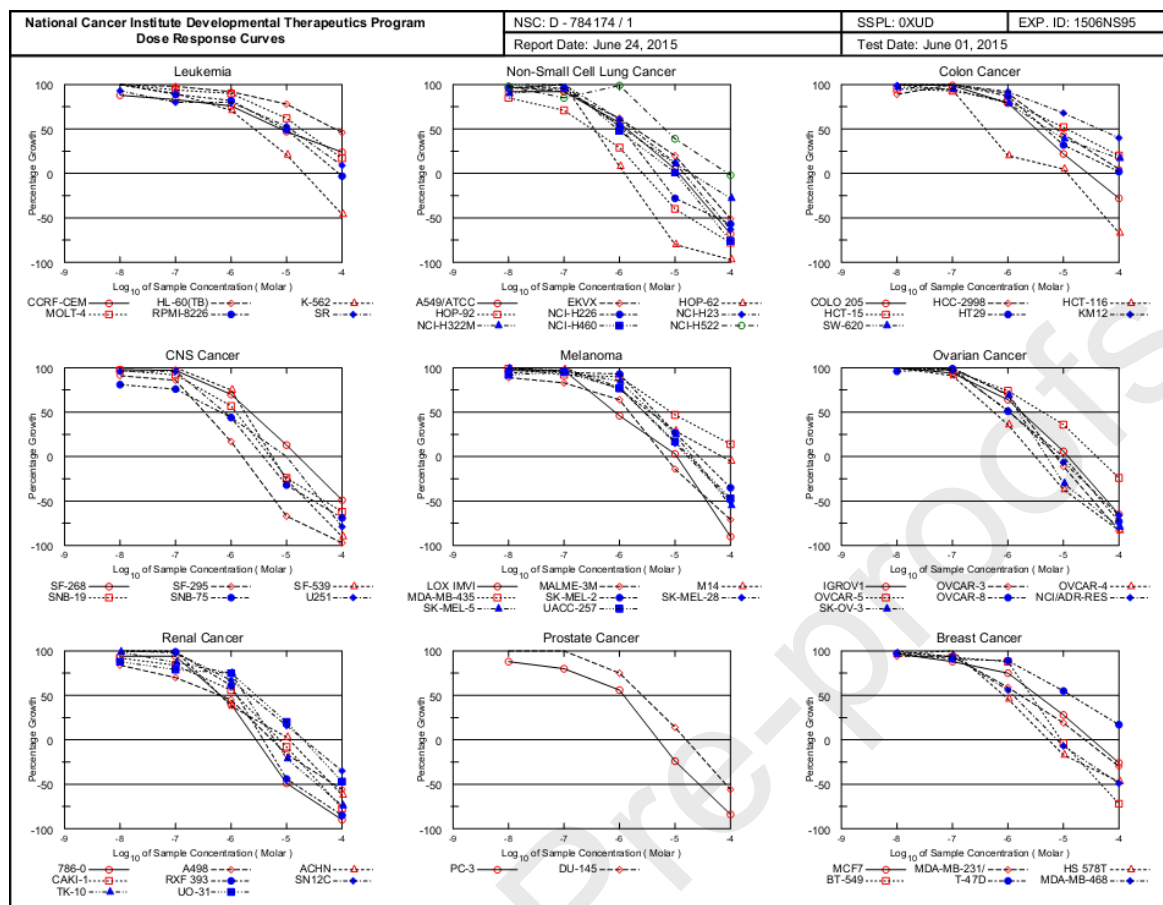


Fig. 4. Concentration-antiproliferative response curves of compound **IVg** against nine different cancer cell lines

2.2.3. Cell viability assay

Cell viability assay was carried out for compounds **IVc**, **IVf**, and **IVg** using human mammary gland epithelial cell line (MCF-10A). MCF-10A cells were treated with the tested compounds for 4 days and 3-(4,5-dimethylthiazol-2-yl)-2,5-diphenyltetrazolium Bromide (MTT) assay was used to assess the cell viability. For all compounds there are no cytotoxic effects and cell viability was greater than 87% at 50 μ M.

2.2.4. Effect of compounds **IVc**, **IVf**, and **IVg** on cancer cell growth

Independently, propidium iodide (PI) fluorescence assay was performed in this analysis to assess the effects of the most active compounds **IVc**, **IVf**, and **IVg** on Panc-1 (pancreas cancer cell line), PaCa-2 (pancreatic carcinoma cell line), HT-29 (colon cancer cell line) and H-460 (lung cancer cell line), while Erlotinib hydrochloride was used as a positive control. The results of the anticancer activity are summarized in **Table 4** and presented as IC₅₀ values. These all compounds were bearing *N*-phenethyl-1*H*-pyrrol-2(3*H*)-one moiety (**Scaffold A**). This class of compounds was found to be more effective compared to other series of compounds having *N*-benzyl-1*H*-pyrrol-2(3*H*)-one (**Scaffold A**) and pyridazin-3(2*H*)-one groups (**Scaffold B**). Compound **IVf** bearing 4-(CH₃)₂N-C₆H₄ moiety was found to be least effective against cancer cell lines. Attachment of 3,4-di-OCH₃-C₆H₃ increased the considerable effect of compound **IVc**. Compound **IVg** bearing 4-Br-C₆H₄ on pyrrole ring showed the most potency and best antiproliferative effects. Compounds **IVc**, **IVf** and **IVg** were therefore subject to further studies to investigate the possible mechanism of action.

Table 4. Antiproliferative activities of compounds **IVc**, **IVf**, and **IVg**.

Compd.	Ar	Cell viability	Antiproliferative activity IC ₅₀ ± SEM (μM)			
			HT-29	PaCa-2	H-460	Panc-1
IVc	3,4-di-OCH ₃ -C ₆ H ₃	89	5.2±1.2	3.8±1.2	6.6±1.1	3.2±1.3
IVf	4-(CH ₃) ₂ N-C ₆ H ₄	91	9.5±2.5	3.7±1.7	ND	5.8±1.6
IVg	4-Br-C ₆ H ₄	87	4.3±0.9	1.5±0.8	2.1±0.7	1.8±0.4
Erlotinib	---		0.05±0.02	0.04±0.02	0.02±0.01	0.06±0.03

2.2.5. Tubulin polymerization inhibitory activity

To confirm whether the observed anticancer activity of the above mentioned compounds is conferred by a microtubule-targeting mechanism, the effect of compounds **IVc**, **IVf**, and **IVg** on tubulin polymerization at concentration of 25 μM using two positive controls, vincristine (a tubulin polymerization inhibitor) and docetaxel (a tubulin polymerization stabilizer) have been evaluated at concentration of 3 μM (**Table 5**). Compounds **IVc** and **IVg** have been shown to be the strongest inhibitors with tubulin polymerization inhibitory effect of (**1012**) and (**929**), respectively comparable to that of vincristine (**805**). It is clear from these results that the molecular target of these compounds was most likely tubulin.

2.2.6. EGFR inhibitory activity

EGFR (Epidermal Growth Factor) is a protein located on the surface of certain cells that allows cells to divide and is characterized by high levels in cancer cells. EGFR inhibitors such as erlotinib bind to and interrupt the tyrosine kinase domain in the epidermal growth factor receptors. **Table 5.** shows the results of EGFR-TK assay for tested compounds **IVc**, **IVf**, and

IVg. From the results, the tested compounds gave a weak EGFR inhibition with IC_{50} of 7.4–9.4 μM .

2.2.7. *BRAF^{V600E} inhibitory activity*

The activity of the newly synthesized compounds **IVc**, **IVf**, and **IVg** against $BRAF^{V600E}$ was tested using an *in vitro* experiment and IC_{50} values were summarized in **Table 5**. *N*-phenethyl-1*H*-pyrrol-2(3*H*)-ones **IVc**, **IVf**, and **IVg** exhibited weak $BRAF^{V600E}$ inhibitory activity with IC_{50} values of 12.6 ± 1.8 , 14.8 ± 2.9 and 16.2 ± 1.7 μM , respectively.

Table 5. Effects of compounds **IVc**, **IVf**, and **IVg** on EGFR, $BRAF^{V600E}$, and Tubulin Polymerization.

Comp.	BRAF inhibition $IC_{50} \pm \text{SEM}$ (μM)	EGFR inhibition $IC_{50} \pm \text{SEM}$ (μM)	(Tubulin) Effect (arbitrary units)
IVc	12.6 ± 1.8	9.4 ± 3.1	1012 ± 244
IVf	14.8 ± 2.9	7.4 ± 1.2	1107 ± 214
IVg	16.2 ± 1.7	9.2 ± 3.5	929 ± 304
Erlotinib	0.05 ± 0.03	0.06 ± 0.03	ND
DPBS	ND	ND	2626 ± 198
Vincristine	ND	ND	805 ± 227
Docetaxel	ND	ND	4625 ± 290

ND: Not determined

2.2.8. Cell cycle analysis and apoptosis detection

2.2.8.1. Cell cycle analysis

Studies have been conducted on the impact of **IVg** compound on the progression of the cell cycle and induction of PaCa-2 apoptosis. PaCa-2 cell was incubated with an IC_{50} concentration of compound **IVg** for 24 h. The cell line was stained with PI/Annexin V and analyzed by flowcytometry using BD FASCC alibur. Results investigation (**Fig. 5**) showed that the percentage of pre-G1 apoptosis induced by compound **IVg** after 24 h of incubation was 24.14%. A high percent of cell accumulation was observed in G2/M phase (32.15%) in PaCa-2 treated with compound **IVg** after 24 h incubation indicating arrest of cell cycle at G2/M phase. PaCa-2 cells treated with compound **IVg** also showed cell aggregation at phase G1 and phase G2 / M after 24 h of incubation but more at phase G2 / M. This suggested that the cell cycle was also arrested during the G2 / M process.

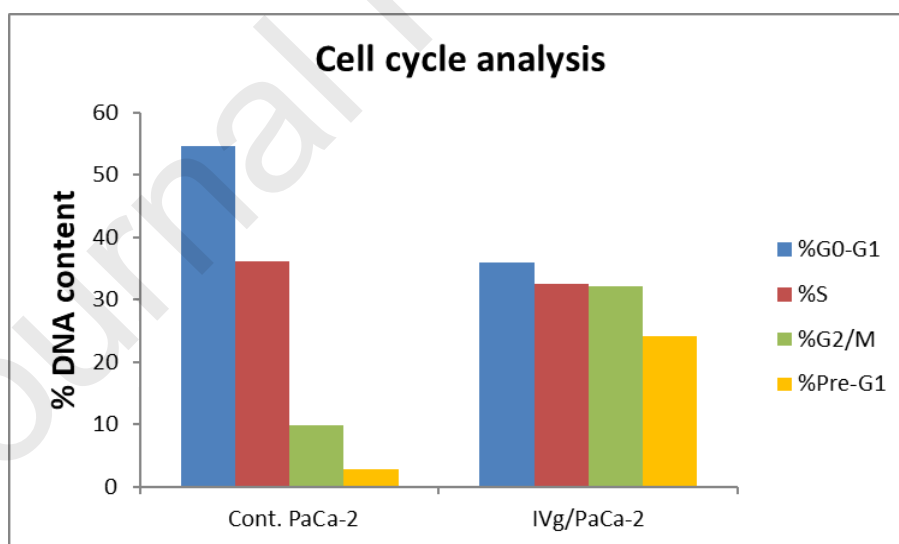


Fig. 5. Cell cycle analysis in MCF-7 cell line treated with compound **IVg**

2.2.8.2. Apoptosis assay

After **IVg** treatment, analysis of the PaCa-2 cell cycle showed pre-G1 apoptosis signalling. Cells were stained with Annexin V/PI and incubated for 24 h to test the ability of **IVg** to induce apoptosis. Early and late apoptosis studies have shown that **IVg** is likely to cause significant apoptosis with 1.98 percent necrosis, (**Fig. 6**).

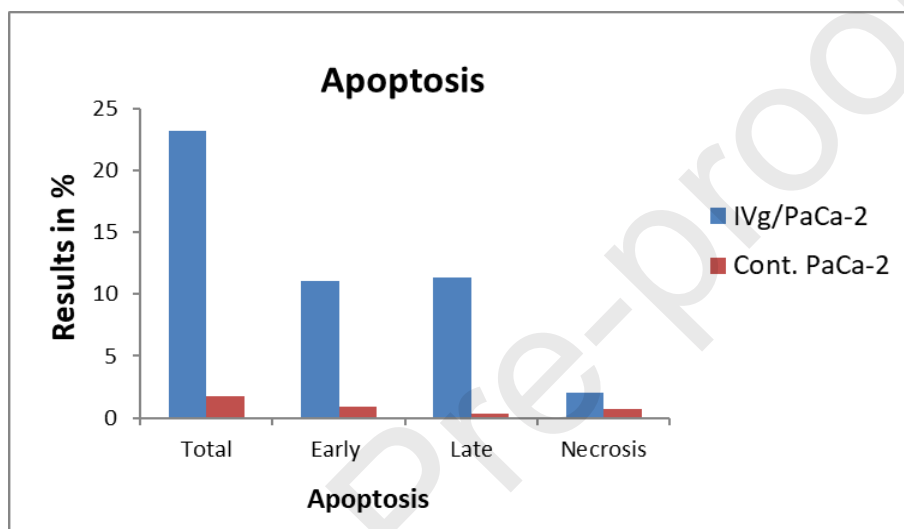


Fig. 6. Percentage of apoptosis and necrosis for compound **IVg** in PaCa-2 cell line

2.3. Docking study into tubulin

In the current work, compounds **IVc**, **IVf**, and **IVg** displayed inhibitory activity against tubulin polymerization, **Table 5**. Accordingly, we have performed a molecular docking study to investigate the potential mechanism which mediate their inhibitory activity against tubulin polymerization. In this study, the binding modes, orientations, and interactions of the compounds **IVc**, **IVf**, and **IVg** were evaluated into colchicine/combretastatin A-4 (CA-4) and vinblastine binding sites. The results of the new compounds were evaluated against the biological results and compared with those of the positive control/native ligands.

2.3.1. Docking study into CA-4 binding site in tubulin

The crystal structure of tubulin protein co-crystallized with CA-4 (PDB code: 5LYJ) [31] was obtained from the Protein Data Bank (<https://www.rcsb.org/structure>). AutoDock 4.2 [32] was used to carry out the docking study. Preparation of protein and ligand files was performed according to the previous reports [33, 34]. The grid and docking parameter files were prepared by AutoDock tools (ADT) following the previous reports [35, 36]. Visualization of the 2/3D binding modes of the docked ligands were performed by Discovery Studio Visualizer [37] and by LigPlot⁺ (v.2.1) [38].

Initially, CA-4 was re-docked into its binding site in tubulin protein to validate the docking procedures. The results of this validation revealed superposition of the re-docked CA-4 over the co-crystallized ligand with RMSD of 0.79 Å. In addition, the re-docked CA-4 displayed the same binding orientation and interactions as those of the co-crystallized ligand, **Fig. 7**.

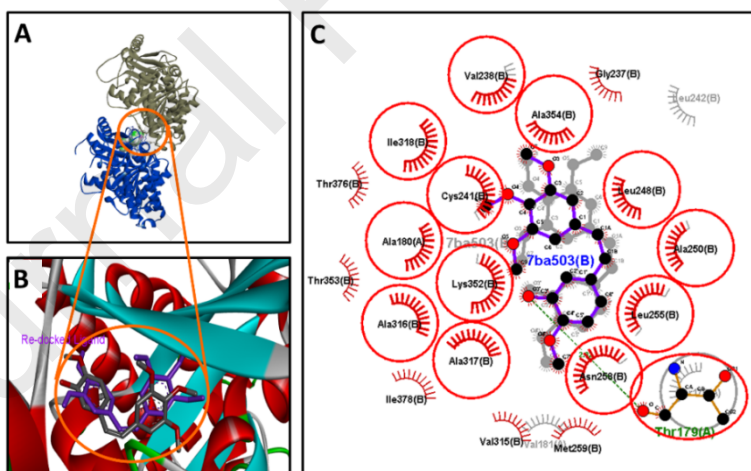


Fig. 7. Binding mode/interactions of redocked/co-crystallized CA-4 into tubulin protein (pdb: 5LYJ): A) binding site of redocked/co-crystallized CA-4 at the α/β interface of tubulin protein, α -subunit colored in grey, β -subunit colored in blue; B) 3D binding mode of the re-docked CA-4 (shown as sticks, colored in purple), superposing with the co-crystallized CA-4 (shown as sticks, colored by element); C) 2D LigPlot view showing superimposition of the redocked CA-4 (shown in purple color), with the co-crystallized CA-4 (shown in gray color) in tubulin, the red circles and ellipses show the amino acid residues which have similar hydrophilic and hydrophobic interactions with the two ligands (re-docked and co-crystallized CA-4).

The binding interactions of combretastatin A-4 (CA-4) into tubulin protein were also investigated to identify the key amino acids in this complex. The results revealed one hydrogen bond with Thr179. Three carbon hydrogen bonds with Val238, Asn258, and Lys352. One pi-sulfur interaction with Met259. Moreover, several hydrophobic interactions of the pi-sigma and pi-alkyl types with Cys241, Leu248, Ala250, Leu255, and Ala316 were also observed.

In addition, the tubulin polymerization inhibitor, colchicine, and compounds **IVc**, **IVf**, and **IVg** which displayed antitubulin activity (**Table 5**) were evaluated for their binding affinities, modes, and interactions into colchicine/CA-4 binding site in tubulin. The results revealed remarkably high binding affinities for the test compounds **IVc**, **IVf**, and **IVg** towards tubulin compared to CA-4 and colchicine,

Table 6.

Table 6. Results of the docking of compounds **IVc**, **IVf**, and **IVg** into Tubulin (5LYJ) in comparison to colchicine and the co-crystallized ligand, CA-4.

Ligand	ΔG_b^a	K_i^b	Amino acids involved in interactions	
			H-bonds/miscellaneous	Hydrophobic
IVc	-12.76	440.76 pM	Asn258, Met259, Asn350,	Cys241, Leu242, Leu248, Ala250, Leu252, Leu255, Ala316, Ile318, Lys352, Ala354, Ile378,
IVf	-12.49	697.53 pM	Cys241, Met259, Asn349	Leu242, Leu248, Ala250, Leu252, Leu255, Ala316, Ile318, Lys352, Ile378.
IVg	-12.99	299.05 pM	Met259	Val181, Cys241, Leu242, Ala250, Leu252, Leu255, Ala316, Ile318, Lys352, Ile378.
CA-4	-8.87	317.06 nM	Thr179, Asn258, Lys352, Val238, Met259	Cys241, Leu248, Ala250, Leu255, Ala316,
Colchicine	-10.80	12.18 nM	Thr179, Val181, Cys241, Asn258, Ala317, Asn350, Lys352.	Cys241, Leu248, Ala250, Leu255, Ala316, Lys352.

^a Binding free energy (kcal/mol); ^b Inhibition constant.

The results revealed binding free energy (ΔG_b) in the range of -12.49 to -12.99 kcal/mol for the three compounds **IVc**, **IVf**, and **IVg** compared to -8.87 kcal/mol for CA-4. Investigation of the binding interactions of the test compounds revealed that they interact mainly by hydrophobic interactions with the amino acids in the binding site of CA-4 in tubulin.

Among the three derivatives, compound **IVg** exhibited the highest binding affinity ($\Delta G_b = -12.99$ kcal/mol) with inhibition constant in the sub-nanomolar range ($K_i = 299.05$ pM). This result was matched with the tubulin polymerization inhibitory activity of the new compounds (**Table 5**). Molecular docking analyses of the best-fit conformation of compound **IVg** revealed the formation of one pi-sulfur interaction with Met259 and several hydrophobic interactions of pi-sigma, alkyl and pi-alkyl with Val181, Cys241, Leu242, Ala250, Leu252, Leu255, Ala316, Ile318, Lys352, and Ile378 amino acids, **Fig. 8**.

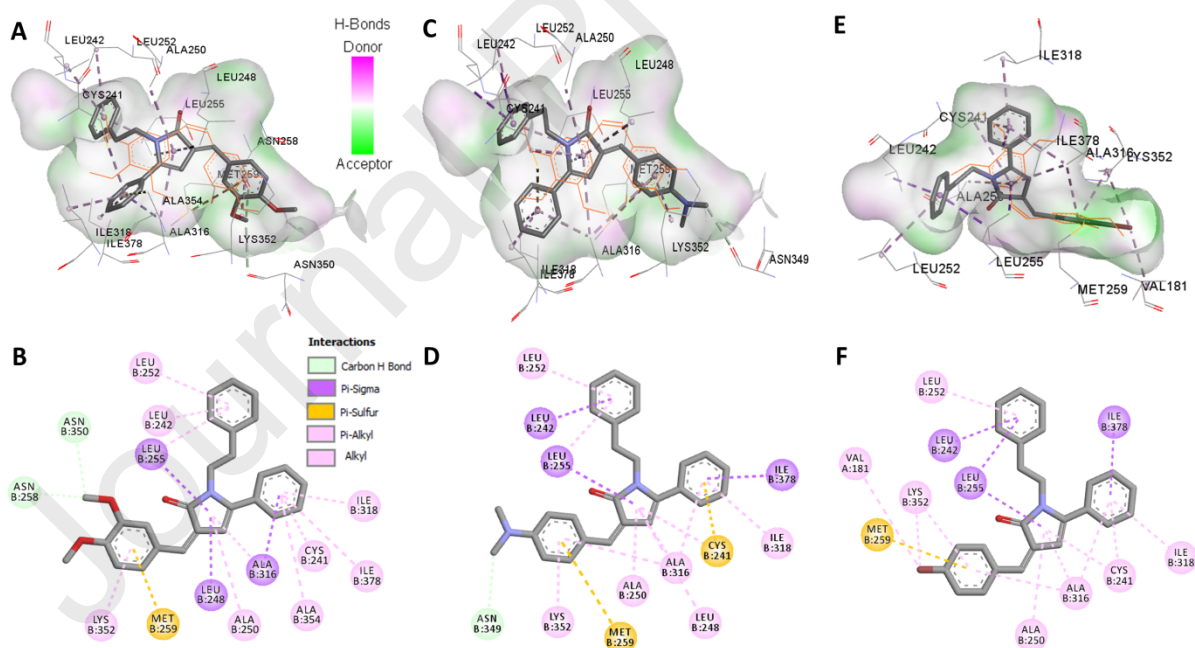


Fig. 8. 2/3D Binding modes/interactions of compound **IVc,f,g** (shown as sticks colored by element) into CA-4 binding site in tubulin (PDB code: 5LYJ), overlaid with the co-crystallized CA-4 shown as orange line, receptor shown as hydrogen bond surface, hydrogen atoms were omitted for clarity: A) 3D binding mode of compound **IVc**; B) 2D binding mode of compound **IVc**; C) 3D binding mode of

compound **IVf**; D) 2D binding mode of compound **IVf**; E) 3D binding mode of compound **IVg**; F) 2D binding mode of compound **IVg**.

Compound **IVc** also displayed high binding affinity ($\Delta G_b = -12.76$ kcal/mol) compared to the native ligand, CA-4 ($\Delta G_b = -8.87$ kcal/mol). Investigation of the binding mode of compound **IVc** revealed two carbon hydrogen bonds with carbonyl oxygen of Asn258 and Asn350 with bond length of 2.03 and 2.80 Å, respectively. One pi-sulfur interaction was also observed between compound **IVc** and Met259. In addition, several hydrophobic interactions of the pi-sigma and pi-alkyl types were formed with Cys241, Leu242, Leu248, Ala250, Leu252, Leu255, Ala316, Ile318, Lys352, and Ile378 in tubulin, **Fig. 8**.

Moreover, compound **IVf** exhibited also higher binding affinity ($\Delta G_b = -12.49$ kcal/mol) than CA-4 and colchicine. Investigation of the binding interactions of compound **IVf** showed one carbon hydrogen bond with the carbonyl oxygen of Asn349 with bond length of 1.90 Å. Two pi-sulfur interaction were also formed with Cys241 and Met259 amino acids. Moreover, several hydrophobic interactions were observed with Leu242, Leu248, Ala250, Leu252, Leu255, Ala316, Ile318, Lys352, and Ile378 in tubulin, **Fig. 8**.

In addition, investigation of the binding modes of compounds **IVc**, **IVf**, and **IVg** revealed that they adopted a *cis*-like conformation and have similar binding orientations with that of CA-4. The phenyl ring (A) in the three compounds superposed over one of the two phenyl rings in CA-4, **Fig. 9**. The double bond between ring A and the pyrrole ring in compounds **IVc**, **IVf**, and **IVg** also superposed with the double bond in CA-4. Moreover, the pyrrole ring in the three compounds occupied the binding site of the trimethoxyphenyl moiety in CA-4.

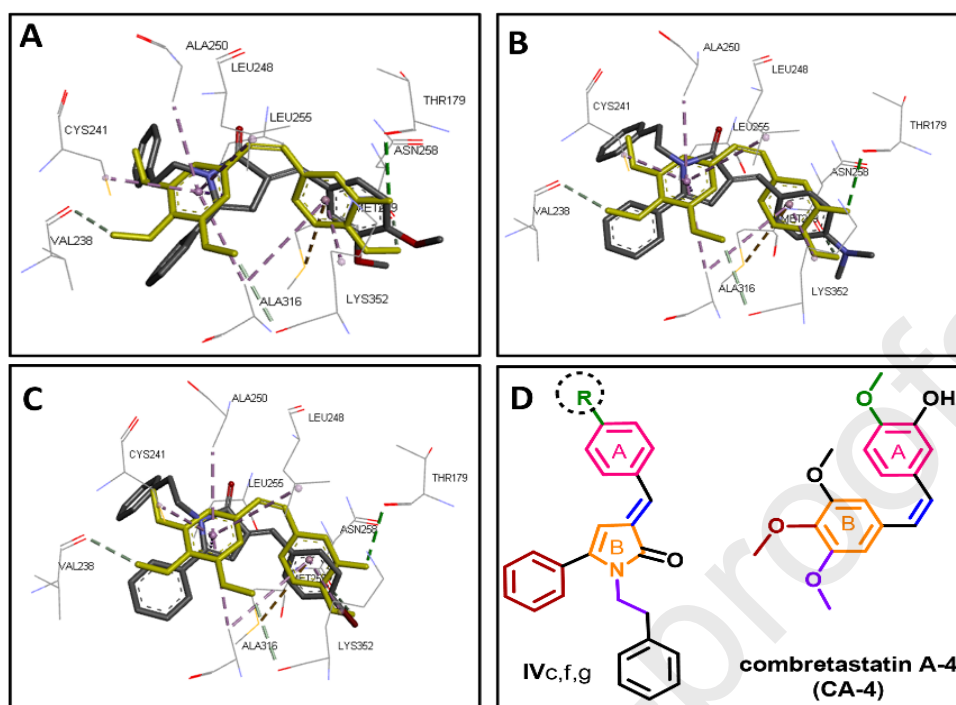


Fig. 9. Binding modes of the compounds **IVc**, **IVf**, and **IVg** and CA-4: A) 3D binding mode of compound **IVc** overlaid with CA-4; B) 3D binding mode of compound **IVf** overlaid with CA-4; C) 3D binding mode of compound **IVg** overlaid with CA-4; D) 2D plot of compounds **IVc**, **IVf**, and **IVg** and CA-4 showing the pharmacophoric groups which superpose over each other and have equivalent binding interaction in tubulin.

2.3.2. Docking study into vinblastine binding site in tubulin

To investigate if the new compounds could inhibit tubulin polymerization through their binding to vinblastine binding site in tubulin, a molecular docking study was also performed. Compounds **IVc,f,g** were docked into vinblastine binding site and compared with vinblastine (VLB) and vincristine. Validation of this study was performed by re-docking the native ligand, VLB into tubulin. The results revealed superposition of the re-docked vinblastine over the co-crystallized ligand with RMSD of VLB is 0.65 Å. Investigation of the binding interactions of the re-docked vinblastine showed similar interactions with those of the co-crystallized ligand, **Fig. 10**.

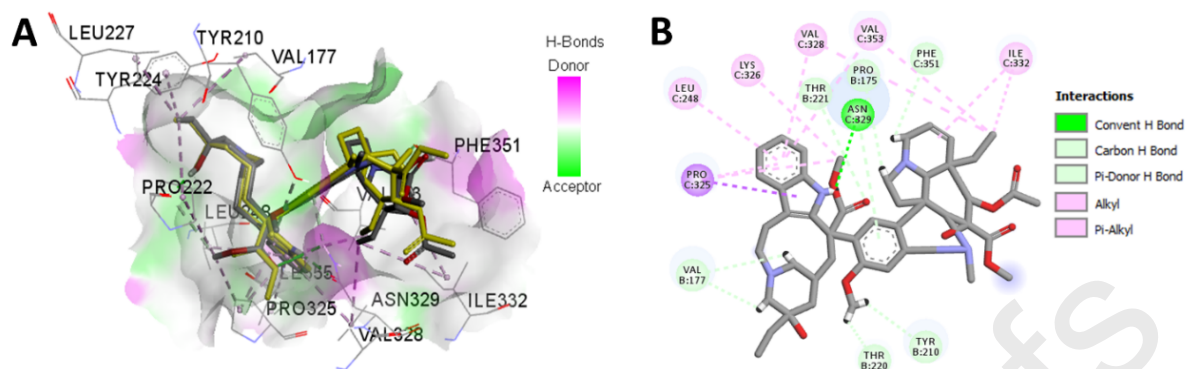


Fig. 10. A) 3D Binding mode of the redocked vinblastine (shown as sticks colored by element) into vinblastine binding site in tubulin (PDB code: 5J2T), overlaid with the co-crystallized ligand shown as yellow sticks, receptor shown as hydrogen bond surface, hydrogen atoms were omitted for clarity; B) 2D binding mode of co-crystallized vinblastine showing different types of interactions with tubulin.

The new compounds **IVc,f,g** and vincristine were docked into the binding site of vinblastine. The results were presented in **Table 7**.

Table 7. Results of the docking of compounds **IVc**, **IVf**, and **IVg** into vinblastine binding site in tubulin (5J2T) in comparison to the co-crystallized ligand, vinblastine.

Ligand	ΔG_b^a	K_i^b	Amino acids involved in interactions	
			H-bonds/miscellaneous	H-bonds/miscellaneous
IVc	-8.60	498.61 nM	Ser178, Tyr210, Thr220, Lys326, Asn329	Val177, Thr221, Pro222, Leu227, Pro325
IVf	-8.75	383.72 nM	Ser178, Thr220, Lys326	Pro222, Leu227
IVg	-8.85	326.07 nM	Thr223	Val177, The221, Pro222, Leu227, Pro325, Lys326
VLB	-13.54	119.27 pM	Pro175, Val177, Tyr210, Thr220, Thr221, An329, Phe351,	Leu248, Pro325, Lys326, Val328, Ile332, Val353
Vincristine	-13.94	60.11 pM	Pro175, Lys176, Ser178, Tyr210, Pro222, Asn329, Lys336	Val177, Tyr224, Leu227, Pro325, Val328, Ile332, Val353

^a Binding free energy (kcal/mol), ^b Inhibition constant

The results revealed very weak binding affinities of the three compounds **IVc**, **IVf**, and **IVg** compared to both vincristine and vinblastine, **Table 7**. Moreover, the calculated K_i values of compounds **IVc**, **IVf**, and **IVg** were 5425-8295 time higher than the calculated K_i value of vincristine. These results are not in concordance with the biological results (**Table 5**). For example, compound **IVg** which showed tubulin polymerization inhibitory activity comparable with that of vincristine. However, the K_i value of compound **IVg** was 5425 higher than that of vincristine. In addition, investigation of the binding interactions of the new compounds with amino acids in VLB binding site revealed the absence of many of the essential binding interactions which were observed with both vinblastine and vincristine, **Table 7**. These results suggested that the inhibitory effect of the new compounds could not be mediated by their binding to the VLB binding site.

3. CONCLUSION

Thirty-five new substituted Combretastatin (CA-4) analogues with Pyrrol-2-one, Pyridazin-3(2*H*)-one and Pyridazin-3(2*H*)-one/oxime core were synthesized and tested by NCI for their antiproliferative activity. Compounds **IVc**, **IVg** and **IVf** showed excellent inhibitory properties on a broad range of cancer cell lines, and tubulin polymerization assays revealed significant inhibitory effects on tubulin assembly for these compounds. This mechanism of action is further supported by docking experiments, which showed that all tested compounds fit well to the colchicine binding site of tubulin. Interestingly, compounds **IVa-g** possessing *N*-phenethyl-1*H*-pyrrol-2(3*H*)-one were more active than **IIIb-d** possessing *N*-benzyl-1*H*-pyrrol-2(3*H*)-one which directly reflects the influences of *N*-phenethyl moiety on the antiproliferative activity of the title scaffold. Docking study of compounds **IVc**, **IVf** and **IVg** revealed nice fitting into CA-4 binding site in tubulin and absence of any steric clashes or unfavorable interactions. The three compounds exhibited extremely higher binding affinities ($\Delta G_b = -12.49$ to -12.99 kcal/mol) toward tubulin than CA-4 (-8.87 kcal/mol). Investigation of the binding modes of the three compounds **IVc**, **IVf** and **IVg** revealed that they interacted mainly through hydrophobic interactions and adopted binding orientations like the binding orientation of CA-4. The *N*-phenethyl-1*H*-pyrrol-2(3*H*)-one derivatives **IVc**, **IVf** and **IVg** are novel promising targeted anticancer tubulin polymerization inhibitors that may participate efficiently in cancer chemotherapy after optimization.

4- Experimental

4.1 Chemistry

General Details. See Appendix A

3-benzoyl propionic acid **I** [28], 5-phenylfuran-2(3*H*)-ones **IIa-g** [29] and 4-(4-Methoxybenzyl)-6-phenylpyridazin-3(2*H*)-one **Va** [30] were synthesized according to reported literatures.

4.1.1. General procedure for synthesis of substituted Pyrrol-2(3*H*)-ones **IIIb-g** and **IVa-g**

A mixture of the corresponding furanone **IIa-g** (0.003 mol) and benzylamine or 2-phenyl ethylamine (0.004 mol) in absolute ethanol (30 ml) was heated at reflux for 3h. The reaction mixture was concentrated, and the formed precipitate was filtered off, washed with petroleum ether, affording the corresponding Pyrrole-2(3*H*)-ones **IIIb-g** and **IVa-g**, respectively.

4.1.1.1. 1-Benzyl-3-(3-methoxybenzylidene)-5-phenyl-1*H*-pyrrol-2(3*H*)-one (**IIIb**)

White powder, 0.63 g (76 % yield), mp = 167-169°C, IR (cm⁻¹): 3052 (CH aromatic), 2920 (CH aliphatic), 1667 (C=O), 1636 (C=C). ¹H NMR (400 MHz, DMSO-*d*₆) δ 7.37–7.23 (m, 7H, Ar-H), 7.21–7.08 (m, 7H, Ar-H), 6.93 (dd, *J* = 8.2, 2.5 Hz, 1H, Ar-H), 6.82 (s, 1H, olefinic H), 4.36 (d, *J* = 15.3 Hz, 1H, CH₂), 4.14 (d, *J* = 15.3 Hz, 1H, CH₂), 3.76 (s, 3H, OCH₃) ¹³C NMR (101 MHz, DMSO-*d*₆) δ 167.9, 159.4, 143.4, 138.2, 136.5, 130.3, 129.9, 129.3, 128.2, 127.9, 127.7, 126.4, 125.5, 121.7, 114.8, 114.6, 89.4, 55.1, 44.4, 43.4. HRESI-MS *m/z* calcd for [M+H]⁺: 368.1645, found: 368.1637.

4.1.1.2. 1-Benzyl-3-(3,4-dimethoxybenzylidene)-5-phenyl-1*H*-pyrrol-2(3*H*)-one (**IIIc**)

White powder, 0.94 g (79 % yield), mp = 162-164°C, IR (cm⁻¹): 3040 (CH aromatic), 2930 (CH aliphatic), 1671 (C=O), 1636 (C=C). ¹H NMR (400 MHz, DMSO-*d*₆) δ 7.38–7.24 (m, 6H, Ar-H),

7.23–7.10 (m, 7H, Ar-H), 6.99 (d, $J = 8.8$ Hz, 1H, Ar-H), 6.81 (s, 1H, olefenic H), 4.35 (d, $J = 15.3$ Hz, 1H, CH₂), 4.13 (d, $J = 15.3$ Hz, 1H, CH₂), 3.77 (s, 6H, 2OCH₃).¹³C NMR (101 MHz, DMSO-*d*₆) δ 168.7, 149.9, 149.2, 144.1, 138.8, 129.9, 128.6, 128.5, 128.3, 128.2, 128.1, 127.8, 126.8, 126.0, 123.3, 113.4, 112.3, 89.8, 56, 55.9, 44.7, 43.8. HRESI-MS m/z calcd for [M+H]⁺: 398.1751, found:398.1739.

4.1.1.3. 1-Benzyl-5-phenyl-3-(3,4, 5-trimethoxybenzylidene)-1*H*-pyrrol-2(3*H*)-one (III*d*)

White powder, 1.04 g (81 % yield), mp = 147-149°C, IR (cm⁻¹): 3070 (CH aromatic), 2937 (CH aliphatic), 1690 (C=O), 1655 (C=C). ¹H NMR (400 MHz, DMSO-*d*₆) δ 7.37–7.25 (m, 6H Ar-H,), 7.20–7.13 (m, 5H, Ar-H), 6.82 (m, 3H, 2Ar-H, olefenic H), 4.34 (d, $J = 15.3$ Hz, 1H, CH₂), 4.13 (d, $J = 15.2$ Hz, 1H, CH₂), 3.79 (s, 6H, 2OCH₃), 3.68 (s, 3H, OCH₃).¹³C NMR (101 MHz, DMSO-*d*₆) δ 168.0, 153.0, 143.5, 138.3, 138.1, 130.8, 129.7, 129.0, 128.2, 127.9, 127.7, 126.4, 125.6, 107.0, 89.5, 60.1, 55.9, 44.0, 43.4. HRESI-MS m/z calcd for [M+H]⁺: 428.1856, found: 428.1844.

4.1.1.4. 1-Benzyl-3-(4-fluorobenzylidene)-5-phenyl-1*H*-pyrrol-2(3*H*)-one (III*e*)

White powder, 0.74 g (70 % yield), mp = 127-129°C, IR (cm⁻¹): 3010 (CH aromatic), 2925 (CH aliphatic), 1675 (C=O), 1646 (C=C). ¹H NMR (400 MHz, DMSO-*d*₆) δ 7.6 –7.57 (m, 2H, Ar-H), 7.36–7.13 (m, 13H, Ar-H), 6.80 (s, 1H, olefenic H), 4.34 (d, $J = 15.3$ Hz, 1H, CH₂), 4.12 (d, $J = 15.3$ Hz, 1H, CH₂). HRESI-MS m/z calcd for [M+H]⁺: 356.1445, found:365.1437.

4.1.1.5. 1-Benzyl-3-(4-(dimethylamino) benzylidene)-5-phenyl-1*H*-pyrrol-2(3*H*)-one (III*f*)

White powder, 0.91 g (80 % yield), mp = 143-145 °C, IR (cm⁻¹): 3020 (CH aromatic), 2930 (CH aliphatic), 1675 (C=O), 1632 (C=C). ¹H NMR (400 MHz, DMSO-*d*₆) δ 7.37-7.12 (m, 13H, Ar-H), 6.73-6.70 (m, 3H, 2Ar-H, olefenic H), 4.33 (d, $J = 15.3$ Hz, 1H, CH₂), 4.08 (d, $J = 15.3$ Hz,

1H, CH₂), 2.94 (s, 3H, N (CH₃)₂), 2.93 (s, 3H, N (CH₃)₂). HRESI-MS m/z calcd for [M+H]⁺: 381.1961 found: 381.1952.

4.1.1.6. 1-Benzyl-3-(4-bromobenzylidene)-5-phenyl-1H-pyrrol-2(3H)-one (IIIg)

White powder, 0.87 g (70 % yield), mp = 217-219°C, IR (cm⁻¹): 3020 (CH aromatic), 2910 (CH aliphatic), 1682 (C=O), 1631 (C=C). ¹H NMR (400 MHz, DMSO-*d*₆) δ 7.61-7.57 (m, 2H, Ar-H), 7.52-7.48 (m, 2H, Ar-H), 7.36-7.24 (m, 6H, Ar-H), 7.20-7.12 (m, 5H, Ar-H), 6.82 (s, 1H, olefinic H), 4.34 (d, *J* = 15.2 Hz, 1H, CH₂), 4.13 (d, *J* = 15.2 Hz, 1H, CH₂). HRESI-MS m/z calcd for [M+H]⁺: 416.0645, found: 416.0612.

4.1.1.7. 3-(4-Methoxybenzylidene)-1-phenethyl-5-phenyl-1H-pyrrol-2(3H)-one (IVa)

White powder, 0.90 g (79 % yield), mp = 172-174°C, IR (cm⁻¹): 2915 (CH aliphatic), 1676 (C=O), 1632 (C=C). ¹H NMR (400 MHz, DMSO-*d*₆) δ 7.50 (d, *J* = 8.8 Hz, 2H, Ar-H), 7.45 (d, *J* = 7.4 Hz, 2H, Ar-H), 7.41-7.39 (m, 2H, Ar-H), 7.37-7.30 (m, 2H, Ar-H), 7.23 (t, *J* = 7.4 Hz, 2H, Ar-H), 7.17-7.13 (m, 1H, Ar-H), 7.01 (d, *J* = 8.7 Hz, 2H, Ar-H), 6.98 (d, *J* = 8.7 Hz, 2H, Ar-H), 6.81 (s, 1H, olefinic H), 3.77 (s, 3H, OCH₃), 3.35 (ddd, *J* = 13.4, 11.5, 5.2 Hz, 1H, NCH₂CH₂), 3.05 (ddd, *J* = 13.4, 11.5, 5.2 Hz, 1H, NCH₂CH₂), 2.80 (ddd, *J* = 13.4, 11.5, 5.2 Hz, 1H, NCH₂CH₂), 2.55 (ddd, *J* = 13.4, 11.5, 5.2 Hz, 1H, NCH₂CH₂). ¹³C NMR (101 MHz, DMSO-*d*₆) δ 167.8, 159.6, 143.8, 139.2, 131.2, 128.7, 128.4, 128.4, 128.3, 127.8, 127.8, 127.3, 126.1, 125.5, 114.3, 89.3, 55.2, 44.5, 41.7, 34.6. HRESI-MS m/z calcd for [M+H]⁺: 382.1802, found: 382.1789.

4.1.1.8. 3-(3-Methoxybenzylidene)-1-phenethyl-5-phenyl-1H-pyrrol-2(3H)-one (IVb)

White powder, 0.84 g (74 % yield), mp = 197-199°C, IR (cm⁻¹): 2910 (CH aliphatic), 1662 (C=O), 1632 (C=C). ¹H NMR (400 MHz, DMSO-*d*₆) δ 7.47-7.44 (m, 2H, Ar-H), 7.42-7.39 (m,

2H, Ar-H), 7.35–7.31 (m, 3H, Ar-H), 7.23 (t, $J = 7.2$ Hz, 2H, Ar-H), 7.17–7.11 (m, 2H, Ar-H), 7.08 (s, 1H, Ar-H), 7.04 – 7.02 (m, 2H, Ar-H), 6.95–6.92 (m, 1H, Ar-H), 6.84 (s, 1H, olefenic H), 3.77 (s, 3H, OCH₃), 3.35 (ddd, $J = 13.4, 11.5, 5.2$ Hz, 1H, NCH₂CH₂), 3.05 (ddd, $J = 13.4, 11.5, 5.2$ Hz, 1H, NCH₂CH₂), 2.80 (ddd, $J = 13.4, 11.5, 5.2$ Hz, 1H, NCH₂CH₂), 2.56 (ddd, $J = 13.4, 11.5, 5.2$ Hz, 1H, NCH₂CH₂). ¹³C NMR (101 MHz, DMSO-*d*₆) δ 167.5, 159.4, 143.6, 139.2, 136.5, 130.4, 129.9, 129.0, 128.4, 128.4, 128.3, 127.9, 126.2, 125.5, 121.7, 114.8, 114.6, 89.3, 55.1, 44.4, 41.7, 34.5. HRESI-MS m/z calcd for [M+H]⁺: 382.1802, found: 382.1787.

4.1.1.9. 3-(3,4-Dimethoxybenzylidene)-1-phenethyl-5-phenyl-1H-pyrrol-2(3H)-one (IVc)

White powder, 0.96 g (78 % yield), mp = 193-195°C, IR (cm⁻¹): 3020 (CH aromatic), 2934 (CH aliphatic), 1676 (C=O). 1632 (C=C), ¹H NMR (400 MHz, DMSO-*d*₆) δ 7.47–7.38 (m, 4H, Ar-H), 7.34–7.29 (m, 2H, Ar-H), 7.23 (t, $J = 7.4$ Hz, 2H, Ar-H), 7.17–7.11 (m, 3H, Ar-H), 7.04-6.98 (m, 3H, Ar-H), 6.80 (s, 1H, olefenic H), 3.78 (s, 6H, 2OCH₃), 3.36 (ddd, $J = 13.4, 11.5, 5.2$ Hz, 1H, NCH₂CH₂), 3.05 (ddd, $J = 13.4, 11.5, 5.2$ Hz, 1H, NCH₂CH₂), 2.80 (ddd, $J = 13.4, 11.5, 5.2$ Hz, 1H, NCH₂CH₂), 2.55 (ddd, $J = 13.4, 11.5, 5.2$ Hz, 6.4 Hz, 1H, NCH₂CH₂). ¹³C NMR (101 MHz, DMSO-*d*₆) δ 167.8, 149.4, 148.7, 143.8, 139.2, 129.2, 128.4, 128.4, 128.3, 128.1, 127.8, 127.5, 126.1, 125.5, 122.8, 112.9, 111.8, 89.3, 55.5, 55.5, 44.3, 41.7, 34.6. HRESI-MS m/z calcd for [M+H]⁺: 412.1907, found: 412.1894.

4.1.1.10. 1-Phenethyl-5-phenyl-3-(3,4, 5-trimethoxybenzylidene)-1H-pyrrol-2(3H)-one (IVd)

White powder, 1.38 g (80 % yield), mp = 187-189°C, IR (cm⁻¹): 3010 (CH aromatic), 2935 (CH aliphatic), 1671 (C=O). 1632 (C=C), ¹H NMR (400 MHz, DMSO-*d*₆) δ 7.49–7.37 (m, 4H, Ar-H), 7.37–7.27 (m, 2H, Ar-H), 7.27–7.20 (m, 2H, Ar-H), 7.20–7.11 (m, 1H, Ar-H), 7.0 – 6.98 (m, 2H, Ar-H), 6.82 (m, 3H, 2Ar-H, olefenic H), 3.79 (s, 6H, 2OCH₃), 3.67 (s, 3H, OCH₃), 3.36 (ddd, $J = 13.4, 11.5, 5.2$ Hz, 1H, NCH₂CH₂), 3.05 (ddd, $J = 13.4, 11.5, 5.2$ Hz, 1H, NCH₂CH₂), 2.79

(ddd, $J = 13.4, 11.5, 5.2$ Hz, 1H, NCH₂CH₂), 2.55 (ddd, $J = 13.4, 11.5, 5.2$ Hz, 1H, NCH₂CH₂).
¹³C NMR (101 MHz, DMSO-*d*₆) δ 167.6, 153.0, 143.7, 139.2, 138.1, 130.8, 129.4, 129.2, 128.4, 128.4, 128.3, 127.9, 126.1, 125.6, 107.0, 89.3, 60.1, 55.9, 44.1, 41.7, 34.5. HRESI-MS m/z calcd for [M+H]⁺: 442.2013, found: 442.2001.

4.1.1.11. 3-(4-Fluorobenzylidene)-1-phenethyl-5-phenyl-1*H*-pyrrol-2(3*H*)-one (IVe)

White powder, 0.74 g (67 % yield), mp = 167-169°C, IR (cm⁻¹): 3027 (CH aromatic), 2950 (CH aliphatic), 1671 (C=O), 1633 (C=C), ¹H NMR (400 MHz, DMSO-*d*₆) δ 7.66 – 7.58 (m, 2H, Ar-H), 7.48 – 7.43 (m, 2H, Ar-H), 7.42- 7.38 (m, 2H, Ar-H), 7.35 – 7.25 (m, 2H, Ar-H), 7.24-7.16 (m, 4H, Ar-H), 7.15-7.04 (m, 1H, Ar-H), 7.02-6.84 (m, 2H, Ar-H), 6.83 (s, 1H, olefinic H), 3.38 (ddd, $J = 13.4, 11.5, 5.2$ Hz, 1H, NCH₂CH₂), 3.06 (ddd, $J = 13.4, 11.5, 5.2$ Hz, 1H, NCH₂CH₂), 2.79 (ddd, $J = 13.4, 11.5, 5.2$ Hz, 1H, NCH₂CH₂), 2.56 (ddd, $J = 13.4, 11.5, 5.2$ Hz, 1H, NCH₂CH₂). HRESI-MS m/z calcd for [M+H]⁺: 370.1602, found: 370.1591.

4.1.1.12. 3-(4-(Dimethylamino)benzylidene)-1-phenethyl-5-phenyl-1*H*-pyrrol-2(3*H*)-one (IVf)

White powder, 0.92 g (78 % yield), mp = 183-185°C, IR (cm⁻¹): 3020 (CH aromatic), 2950 (CH aliphatic), 1663 (C=O), 1631 (C=C). ¹H NMR (400 MHz, DMSO-*d*₆) δ 7.46–7.30 (m, 7H, Ar-H), 7.25–7.13 (m, 4H, Ar-H), 7.04–7.01(m, 2H, Ar-H), 6.74–6.71 (m, 3H, 2Ar-H, olefinic H), 2.94 (s, 3H, N(CH₃)₂), 2.93 (s, 3H, N(CH₃)₂) 3.36 (ddd, $J = 13.4, 11.5, 5.2$ Hz, 1H, NCH₂CH₂), 3.02 (ddd, $J = 13.4, 11.5, 5.2$ Hz, 1H, NCH₂CH₂), 2.78 (ddd, $J = 13.4, 11.5, 5.2$ Hz, 1H, NCH₂CH₂), 2.55 (ddd, $J = 13.4, 11.5, 5.2$ Hz, 1H, NCH₂CH₂). HRESI-MS m/z calcd for [M+H]⁺: 395.2118, found: 395.2109.

4.1.1.13. 3-(4-Bromobenzylidene)-1-phenethyl-5-phenyl-1*H*-pyrrol-2(3*H*)-one (IVg)

White powder, 0.85 g (68 % yield), mp = 226-228°C, IR (cm⁻¹): 3027 (CH Aromatic), 2950 (CH Aliphatic), 1671 (C=O), 1632 (C=C). ¹H NMR (400 MHz, DMSO-*d*₆) δ 7.60-7.50 (dd, *J* = 8.5, 1.7 Hz, 4H, Ar-H), 7.46-7.21 (m, 8H, Ar-H), 7.18–7.15 (m, 1H, Ar-H), 7.04-7.01(m, 2H, Ar-H), 6.85 (s, 1H, olefinic H), 3.37 (ddd, *J* = 13.4, 11.5, 5.2 Hz, 1H, NCH₂CH₂), 3.05 (ddd, *J* = 13.4, 11.5, 5.2 Hz, 1H, NCH₂CH₂), 2.78 (ddd, *J* = 13.4, 11.5, 5.2 Hz, 1H, NCH₂CH₂), 2.55 (ddd, *J* = 13.4, 11.5, 5.2 Hz, 1H, NCH₂CH₂). HRESIMS *m/z* calcd for [M+H]⁺: 430.0801, found: 430.0789.

4.1.2. General procedure for the synthesis of substituted pyridazin-3(2*H*)-ones (Va-f)

A mixture of furanones **IIa-f** (0.003 mol) and hydrazine mono hydrate 98 % (2 ml) in absolute ethanol (10 ml) was heated at reflux for 3 h. After cooling the reaction mixture poured onto crushed ice and the formed precipitate was filtered off, washed, dried, and crystallized from methanol to give the corresponding pyridazinone **Va-f**.

4.1.2.1. 4-(3-Methoxybenzyl)-6-phenylpyridazin-3(2*H*)-one (Vb)

White powder, 0.69 g (79 % yield), mp = 201-203°C, IR (cm⁻¹): 3280 (NH), 3070 (CH aromatic), 2901(CH aliphatic), 1663 (C=O), 1601 (C=C). ¹H NMR (400 MHz, DMSO-*d*₆) δ 13.18 (s, 1H, NH), 7.85 (s, 1H, Ar-H), 7.79 (d, 2H, *J* = 8 Hz, Ar-H), 7.48–7.38 (m, 3H, Ar-H), 7.21 (t, *J* = 7.9 Hz, 1H, Ar-H), 6.95–6.91 (m, 2H, Ar-H), 6.79 (dd, *J* = 8.2, 2.6 Hz, 1H, Ar-H), 3.85 (s, 2H, CH₂), 3.72 (s, 3H, OCH₃). ¹³C NMR (101 MHz, DMSO-*d*₆) δ 160.7, 159.3, 144.0, 142.6, 139.7, 134.9, 129.4, 129.1, 128.9, 128.1, 125.6, 121.2, 114.9, 111.7, 54.9, 35.1. HRESIMS *m/z* calcd for [M+H]⁺: 293.1285, found: 293.1277.

4.1.2.2. 4-(3, 4-Dimethoxybenzyl)-6-phenylpyridazin-3(2H)-one (Vc)

White powder, 0.79 g (82 % yield), mp =157-159°C, (cm⁻¹): 3500 (NH), 3090 (CH Aromatic), 2964 (CH Aliphatic), 1655 (C=O), 1605 (C=C). ¹H NMR (400 MHz, DMSO-*d*₆) δ 13.14 (s, 1H, NH), 7.77 (d, *J* = 6.8 Hz, 3H, Ar-H), 7.48-7.38 (m, 3H, Ar-H), 6.99 (s, 1H, Ar-H), 6.86 (d, *J* = 8Hz, 2H, Ar-H) , 3.86 – 3.65 (m, 8H, 2OCH₃, CH₂). ¹³C NMR (101 MHz, DMSO-*d*₆) δ 160.7, 148.7, 147.5, 144.0, 143.1, 135.0, 130.4, 129.1, 128.9, 127.7, 125.6, 121.0, 113.1, 111.9, 55.5, 34.7. HRESI-MS m/z calcd for [M+H]⁺: 323.1390, found: 323.1390.

4.1.2.3. 6-Phenyl-4-(3,4,5-trimethoxybenzyl) pyridazin-3(2H)-one (Vd)

White powder, 1.06 g (84 % yield), mp = 148-150°C, IR (cm⁻¹): 3269 (NH), 3050 (CH aromatic), 2935(CH aliphatic), 1676 (C=O), 1632 (C=C). ¹H NMR (400 MHz, DMSO-*d*₆) δ 13.18 (s, 1H, NH), 7.83–7.78 (m, 3H, Ar-H), 7.47-7.38 (m, 3H, Ar-H), 6.71 (s, 2H, Ar-H), 3.81 (s, 2H, CH₂), 3.74 (s, 6H, 2OCH₃), 3.63 (s, 3H, OCH₃). ¹³C NMR (101 MHz, DMSO-*d*₆) δ 160.8, 152.8, 144.1, 142.7, 136.2, 135.0, 133.8, 129.1, 128.9, 127.9, 125.7, 106.5, 60.0, 55.9, 35.4. HRESI-MS m/z calcd for [M+H]⁺: 353.1496, found: 353.1487.

4.1.2.4. 4-(4-Fluorobenzyl)-6-phenylpyridazin-3(2H)-one (Ve)

White powder, 0.67 g (79 % yield), mp = 131-133°C, IR (cm⁻¹): 3320 (NH), 3090 (CH aromatic), 2936 (CH aliphatic), 1652 (C=O), 1631 (C=C). ¹H NMR (400 MHz, DMSO-*d*₆) δ 13.17 (s, 1H, NH), 7.87 (s, 1H, Ar-H), 7.80 (d, *J* = 8.2 Hz, 2H, Ar-H), 7.48–7.38 (m, 5H, Ar-H), 7.11 (t, *J* = 8.7 Hz, 2H, Ar-H), 3.86 (s, 2H, CH₂). HRESI-MS m/z calcd for [M+H]⁺: 281.1085, found:281.1077.

4.1.2.5. 4-(4-(Dimethyl amino) benzyl)-6-phenylpyridazin-3(2H)-one (Vf)

White powder, 0.70g (76 % yield), mp = 212-214°C, IR (cm⁻¹): 3300 (NH), 3090 (CH aromatic), 2995 (CH aliphatic), 1661 (C=O), 1633 (C=C), ¹H NMR (400 MHz, DMSO-*d*₆) δ 13.10 (s, 1H, NH), 7.79–7.77 (m, 3H, Ar-H), 7.49–7.42 (m, 3H, Ar-H), 7.15 (d, *J* = 8 Hz, 2H, Ar-H), 6.67 (d, *J* = 8 Hz, 2H, Ar-H), 3.73 (s, 2H, CH₂), 2.84 (s, 3H, N(CH₃)₂), 2.83 (s, 3H, N(CH₃)₂). HRESI-MS m/z calcd for [M+H]⁺: 306.1601, found:306.1593.

4.1.3. General procedure for synthesis of *N*-alkylated pyridazinones (VIb-f) and (VIIa-f)

The appropriate pyridazinone **Va-f** (0.001 mol) was stirred overnight at room temperature with benzyl bromide or phenacyl bromide (0.001 mol) in sodium ethoxide (0.001 Mole). The reaction mixture was poured onto cold water and the formed precipitate was filtered off, washed with water, and crystalized from methanol to give compounds **VIb-f** and **VIIa-f**, respectively.

4.1.3.1. 2-Benzyl-4-(3-methoxybenzyl)-6-phenylpyridazin-3(2H)-one (VIb)

White powder, 0.24g (62 % yield), mp = 125-127°C, IR (cm⁻¹): 3061 (CH aromatic), 2958 (CH aliphatic), 1648 (C=O), 1608 (C=C). ¹H NMR (400 MHz, DMSO-*d*₆) δ 7.88 (s, 1H, Ar-H), 7.81 (d, *J* = 8.0 Hz, 2H, Ar-H), 7.50-7.42 (m, 3H, Ar-H), 7.37-7.32 (m, 5H, Ar-H), 7.30–7.20 (m, 1H, Ar-H), 6.92 (t, *J* = 12.0 Hz, 2H, Ar-H), 6.80 (d, *J* = 8.0 Hz, 1H, Ar-H), 5.34 (s, 2H, NCH₂), 3.88 (s, 2H, CH₂), 3.71 (s, 3H, OCH₃). HRESI-MS m/z calcd for [M+H]⁺: 383.17540, found: 383.17595.

4.1.3.2. 2-Benzyl-4-(3,4-dimethoxybenzyl)-6-phenylpyridazin-3(2H)-one (VIc)

White powder, 0.27g (65 % yield), mp = 122-124°C, IR (cm⁻¹): 3050 (CH aromatic), 2932 (CH aliphatic), 1655 (C=O), 1611 (C=C). ¹H NMR (400 MHz, DMSO-*d*₆) δ 7.80 (d, *J* = 8.0 Hz, 3H, Ar-H), 7.48–7.45 (m, 3H, Ar-H), 7.38–7.32 (m, 5H, Ar-H), 6.98 (s, 1H, Ar-H), 6.87–6.86 (m,

2H, Ar-H), 5.35 (s, 2H, NCH₂), 3.84 (s, 2H, CH₂), 3.71 (s, 3H, OCH₃), 3.70 (s, 3H, OCH₃). HRESI-MS m/z calcd for [M+H]⁺: 413.18597, found:413.18652.

4.1.3.3. 2-Benzyl-6-phenyl-4-(3,4,5-trimethoxybenzyl)pyridazin-3(2H)-one (VIId)

White powder, 0.30g (68 % yield), mp = 98-100°C, IR (cm⁻¹): 3020 (CH Aromatic), 2960 (CH Aliphatic), 1651 (C=O), 1632 (C=C), ¹H NMR (400 MHz, DMSO-*d*₆) δ 7.87–7.81 (m, 3H, Ar-H), 7.50–7.44 (m, 3H, Ar-H), 7.38-7.28 (m, 5H, Ar-H), 6.68 (s, 2H, Ar-H), 5.36 (s, 2H, NCH₂), 3.84 (s, 2H, CH₂), 3.72 (s, 6H, 2OCH₃), 3.62 (s, 3H, OCH₃). HRESI-MS m/z calcd for [M+H]⁺: 443.19653, found: 443.19708

4.1.3.4. 2-Benzyl-4-(4-fluorobenzyl)-6-phenylpyridazin-3(2H)-one (VIe)

White powder, 0.23g (64 % yield), mp = 127-130°C, IR (cm⁻¹): 3050 (CH aromatic), 2913 (CH aliphatic), 1652 (C=O), 1601 (C=C). ¹H NMR (400 MHz, DMSO-*d*₆) δ 7.91 (s, 1H, Ar-H), 7.82 (d, *J* = 8.1Hz, 2H, Ar-H), 7.50–7.27 (m, 10H, Ar-H), 7.12 (t, *J* = 8.0 Hz, 2H, Ar-H), 5.33 (s, 2H, NCH₂), 3.89 (s, 2H, CH₂). HRESI-MS m/z calcd for [M+H]⁺: 371.1554, found:371.1547.

4.1.3.5. 2-Benzyl-4-(4-(dimethylamino)benzyl)-6-phenylpyridazin-3(2H)-one (VIIf)

White powder, 0.24g (62 % yield), mp = 117-119°C, IR (cm⁻¹): 1632 (C=O), 1606 (C=C). ¹H NMR (400 MHz, DMSO-*d*₆) δ 7.48 (s, 3H, Ar-H), 7.46–7.28 (m, 8H, Ar-H), 7.16 (d, *J* = 8.1Hz, 2H, Ar-H), 6.73–6.65 (m, 2H, Ar-H), 5.33 (s, 2H, NCH₂), 3.77 (s, 2H, CH₂), 2.84 (s, 6H, N(CH₃)₂). HRESI-MS m/z calcd for [M+H]⁺: 396.20704, found: 396.20759.

4.1.3.6. 4-(4-Methoxybenzyl)-2-(2-oxo-2-phenylethyl)-6-phenylpyridazin-3(2H)-one (VIIa)

White powder, 0.27g (65 % yield), mp = 142-144°C, IR (cm⁻¹): 3066 (CH aromatic), 2934 (CH aliphatic), 1702 (CH₂C=O), 1655 (N C=O), 1601 (C=C). ¹H NMR (400 MHz, DMSO-*d*₆) δ 8.08 (d, *J* = 8.0Hz, 2H, Ar-H), 7.96 (s, 1H, Ar-H), 7.83 (d, *J* = 8.0Hz, 2H, Ar-H), 7.73 (t, *J* = 8.0Hz,

1H, Ar-H), 7.60 (t, $J = 8.0\text{Hz}$, 2H, Ar-H), 7.51-7.45 (m, 3H, Ar-H), 7.28 (d, $J = 8.0\text{Hz}$, 2H, Ar-H), 6.87(d, $J = 8.0\text{Hz}$, 2H, Ar-H), 5.75 (s, 2H, COCH₂), 3.85 (s, 2H, CH₂), 3.72 (s, 3H, OCH₃). HRESI-MS m/z calcd for [M+H]⁺: 411.17032, found:411.17087.

4.1.3.7. 4-(3-Methoxybenzyl)-2-(2-oxo-2-phenylethyl)-6-phenylpyridazin-3(2H)-one (VIIf)

White powder, 0.25g (60 % yield), mp = 169-171°C, IR (cm⁻¹): 3053 (CH aromatic), 2936 (CH aliphatic), 1702 (CH₂C=O), 1656 (N C=O), 1600 (C=C). ¹H NMR (400 MHz, DMSO-d₆) δ 8.08 (d, $J = 8.0\text{Hz}$, 2H, Ar-H), 8.01 (s, 1H, Ar-H), 7.84 (d, $J = 8.0\text{Hz}$, 2H, Ar-H), 7.72 (t, $J = 8.0\text{Hz}$, 1H, Ar-H), 7.60 (t, $J = 8.0\text{Hz}$, 1H, Ar-H), 7.49–7.47 (m, 3H, Ar-H), 7.21(t, $J = 8.0\text{Hz}$, 1H, Ar-H), 6.94–6.91(m, 2H), 6.81(d, $J = 8.0\text{Hz}$, 2H, Ar-H), 5.76 (s, 2H, COCH₂), 3.89 (s, 2H, CH₂), 3.72 (s, 3H, OCH₃). HRESI-MS m/z calcd for [M+H]⁺: 411.17033, found:411.17082.

4.1.3.8. 4-(3,4-Dimethoxybenzyl)-2-(2-oxo-2-phenylethyl)-6-phenylpyridazin-3(2H)-one (VIIf)

White powder, 0.28g (65 % yield), mp = 172-174°C, IR (cm⁻¹): 3005 (CH aromatic), 2955 (CH aliphatic), 1698 (CH₂C=O), 1632 (N C=O), 1601 (C=C). ¹H NMR (400 MHz, DMSO-d₆) δ 8.09–6.85 (m, 14H, Ar-H), 5.77 (s, 2H, COCH₂), 3.85 (s, 2H, CH₂), 3.73 (s, 6H, 2OCH₃). HRESI-MS m/z calcd for [M+H]⁺: 441.18021, found:411.17073.

4.1.3.9. 2-(2-Oxo-2-phenylethyl)-6-phenyl-4-(3,4,5-trimethoxybenzyl)pyridazin-3(2H)-one (VIIf)

White powder, 0.31g (66 % yield), mp = 107-109°C, IR (cm⁻¹): 3030 (CH aromatic), 2936 (CH aliphatic), 1696 (CH₂C=O), 1655 (N C=O), 1631 (C=C), ¹H NMR (400 MHz, DMSO-d₆) δ 8.08 (d, $J = 8.0\text{Hz}$, 2H, Ar-H), 7.98 (s, 1H, Ar-H), 7.85–7.83 (m, 2H, Ar-H), 7.73 (t, $J = 8.0\text{Hz}$, 1H, Ar-H), 7.61 (t, $J = 8.0\text{Hz}$, 2H, Ar-H), 7.50–7.47 (m, 3H, Ar-H), 6.69 (s, 2H, Ar-H), 5.78 (s, 2H,

COCH₂), 3.86 (s, 2H, CH₂), 3.75 (s, 6H, 2OCH₃), 3.63 (s, 3H, OCH₃). Anal. Calcd for C₂₈H₂₆N₂O₅ (470.18): C, 71.47; H, 5.57; N, 5.95. Found: C, 71.62; H, 5.64; N, 6.04.

4.1.3.10. 4-(4-Fluorobenzyl)-2-(2-oxo-2-phenylethyl)-6-phenylpyridazin-3(2H)-one (VIIe)

White powder, 0.25g (63 % yield), mp = 142-144°C, IR (cm⁻¹): 3020 (CH aromatic), 2888 (CH aliphatic), 1701 (CH₂C=O), 1651 (N C=O), 1632 (C=C), ¹H NMR (400 MHz, DMSO-d₆) δ 8.08 (d, *J* = 8.0Hz, 2H, Ar-H), 8.04 (s, 1H, Ar-H), 7.85 (d, *J* = 8.0Hz, 2H, Ar-H), 7.73 (t, *J* = 8.0Hz, 1H, Ar-H), 7.60 (t, *J* = 8.0Hz, 2H Ar-H,), 7.51–7.46 (m, 3H, Ar-H), 7.42–7.39(m, 2H, Ar-H), 7.14 (t, *J* = 8.0Hz, 2H Ar-H,), 5.76 (s, 2H, COCH₂), 3.91 (s, 2H, CH₂), HRESI-MS m/z calcd for [M+H]⁺: 399.15033, found: 399.15088.

4.1.3.11. 4-(4-(Dimethylamino)benzyl)-2-(2-oxo-2-phenylethyl)-6-phenylpyridazin-3(2H)-one (VIIIf)

White powder, 0.26g (61 % yield), mp = 173-175°C, IR (cm⁻¹): 3060 (CH aromatic), 2933 (CH aliphatic), 1706 (CH₂C=O), 1659 (N C=O), 1632 (C=C). ¹H NMR (400 MHz, DMSO-d₆) δ 8.08 (d, *J* = 8.0Hz, 2H, Ar-H), 7.91 (s, 1H, Ar-H), 7.82 (d, *J* = 8.0Hz, 2H, Ar-H), 7.73 (t, *J* = 8.0Hz, 1H, Ar-H), 7.60 (t, *J* = 8.0Hz, 2H, Ar-H), 7.46 (t, *J* = 8.0Hz, 3H, Ar-H), 7.17 (d, *J* = 8.0Hz, 2H, Ar-H), 6.67 (d, *J* = 8.0Hz, 2H, Ar-H), 5.74 (s, 2H, COCH₂), 3.79 (s, 2H, CH₂), 2.85 (s, 6H, N(CH₃)₂). HRESI-MS m/z calcd for [M+H]⁺: 424.20012, found: 399.20023.

4.1.4. General procedure for the synthesis of pyridazinone/oxime hybrids (VIIIa-f)

A mixture of appropriate ketones VIIa-f (0.001 mol), hydroxylamine hydrochloride (0.001 Mole) and sodium sulphate anhydrous (0.003 mol) was heated at reflux in absolute ethanol (30 ml) for 6 h. The reaction mixture was poured onto cold water, filtered off, washed with water, and crystalized from aqueous methanol affording the corresponding oximes VIIIa-f.

4.1.4.1. 2-(2-(Hydroxyimino)-2-phenylethyl)-4-(4-methoxybenzyl)-6-phenylpyridazin-3(2H)-one (VIIIa)

White powder, 0.39g (92 % yield), mp = 159-161°C, IR (cm⁻¹): 3223 (OH), 3010 (CH aromatic), 2835 (CH aliphatic), 1635 (C=O), 1592 (C=C). ¹H NMR (400 MHz, DMSO-*d*₆) Major isomer; δ 11.66 (s, 1H, OH), 7.80 (s, 2H, Ar-H), 7.66 (d, *J* = 8.0Hz, 2H, Ar-H), 7.52–7.27(m, 7H, Ar-H), 7.18 (d, *J* = 8.0Hz, 2H, Ar-H), 6.85 (d, *J* = 8.0Hz, 2H, Ar-H), 5.46 (s, 2H, NCH₂), 3.79 (s, 2H, CH₂), 3.72 (s, 3H, OCH₃). Minor isomer; δ 11.17 (s, 1H, OH), 7.80–6.85 (m, 15 H, Ar-H), 5.22 (s, 2H, NCH₂), 3.79 (s, 2H, CH₂), 3.72 (s, 3H, OCH₃). HRESI-MS *m/z* calcd for [M+H]⁺: 426.18122, found: 426.18177.

4.1.4.2. 2-(2-(Hydroxyimino)-2-phenylethyl)-4-(3-methoxybenzyl)-6-phenylpyridazin-3(2H)-one (VIIIb)

White powder, 0.38g (90 % yield), mp = 149-151°C, IR (cm⁻¹): 3285 (OH), 3015 (CH aromatic), 2837 (CH aliphatic), 1632 (C=O), 1594 (C=C). ¹H NMR (400 MHz, DMSO-*d*₆) Major isomer; δ 11.67 (s, 1H, OH), 7.84–6.80 (m, 15H, Ar-H), 5.47 (s, 2H, NCH₂), 3.83 (s, 2H, CH₂), 3.72 (s, 3H, OCH₃). Minor isomer; δ 11.2 (s, 1H, OH), 7.84–6.80 (m, 15H, Ar-H), 5.3 (s, 2H, NCH₂), 3.83 (s, 2H, CH₂), 3.72 (s, 3H, OCH₃). HRESI-MS *m/z* calcd for [M+H]⁺: 426.18122, found: 426.18177.

4.1.4.3. 4-(3,4-dimethoxybenzyl)-2-(2-(hydroxyimino)-2-phenylethyl)-6-phenylpyridazin-3(2H)-one (VIIIc)

White powder, 0.42g (92 % yield), mp = 162-164°C, IR (cm⁻¹): 3270 (OH), 3050 (CH aromatic), 2932 (CH aliphatic), 1644 (C=O), 1593 (C=C). ¹H NMR (400 MHz, DMSO-*d*₆) Major isomer; δ 11.64 (s, 1H, OH), 7.77–7.27 (m, 11H, Ar-H), 6.95–6.74 (m, 3H, Ar-H), 5.46 (s, 2H, NCH₂),

3.73 (s, 2H, CH₂), 3.35 (s, 6H, 2OCH₃). Minor isomer; δ 11.2 (s, 1H, OH), 7.77–6.74 (m, 14 H, Ar-H), 5.24 (s, 2 H, NCH₂), 3.73 (s, 2H, CH₂), 3.35 (s, 6H, 2OCH₃). HRESI-MS m/z calcd for [M+H]⁺: 456.19123, found: 426.19171.

4.1.4.4. 2-(2-(Hydroxyimino)-2-phenylethyl)-6-phenyl-4-(2,3,4-trimethoxybenzyl)pyridazin-3(2H)-one (VIII d)

White powder, 0.46g (94 % yield), mp = 142-145°C, IR (cm⁻¹): 3327 (OH), 3040 (CH aromatic), 2940(CH aliphatic), 1647 (C=O), 1590 (C=C). ¹H NMR (400 MHz, DMSO-d₆) Major isomer; δ 11.66 (s, 1H, OH), 7.82 (s, 1H, Ar-H), 7.67-7.25 (m, 10H, Ar-H), 6.66 (s, 2H, Ar-H), 5.48 (s, 2H, NCH₂), 3.80 (s, 2H, CH₂), 3.73 (s, 6H, 2OCH₃), 3.63 (s, 3H, OCH₃). Minor isomer; δ 11.15 (s, 1H, OH), 7.82–6.66 (m, 13 H, Ar-H), 5.24 (s, 2H, NCH₂), 3.80 (s, 2H, CH₂), 3.73 (s, 6H, 2OCH₃), 3.63 (s, 3H, OCH₃). HRESI-MS m/z calcd for [M+H]⁺: 486.20243, found: 486.20281.

4.1.4.5. 4-(4-Fluorobenzyl)-2-(2-(hydroxyimino)-2-phenylethyl)-6-phenylpyridazin-3(2H)-one (VIII e)

White powder, 0.37g (88 % yield), mp = 157-159°C, IR (cm⁻¹): 3223 (OH), 3057 (CH aromatic), 2950 (CH aliphatic), 1638 (C=O), 1589 (C=C). ¹H NMR (400 MHz, DMSO-d₆) Major isomer; δ 11.66 (s, 1H, OH), 7.87 (s, 1H, Ar-H), 7.68 (d, *J* = 8.0Hz, 2H, Ar-H), 7.50 (d, *J* = 8.0Hz, 2H, Ar-H), 7.43–7.26 (m, 8H, Ar-H), 7.13-7.09 (m, 2H, Ar-H), 5.46(s, 2H, NCH₂), 3.84 (s, 2H, CH₂). Minor isomer; δ 11.16 (s, 1H, OH), 7.82–7.09 (m, 15H, Ar-H), 5.23 (s, 2H, NCH₂), 3.84 (s, 2H, CH₂). HRESI-MS m/z calcd for [M+H]⁺: 414.16123, found: 414.16178.

4.1.4.6. 4-(4-(Dimethylamino)benzyl)-2-((hydroxyimino)-2-phenylethyl)-6-phenylpyridazin-3(2H)-one (VIII f)

White powder, 0.37g (85 % yield), mp = 167-169°C, IR (cm⁻¹): 3219 (OH), 3056 (CH aromatic), 2887 (CH aliphatic), 1636 (C=O), 1591 (C=C). ¹H NMR (400 MHz, DMSO-d₆) Major isomer; δ 11.65 (s, OH), 7.72–7.64(m, 1H, Ar-H), 7.52 (d, *J* = 8.0Hz, 2H, Ar-H), 7.41 (d, *J* = 8.0Hz, 2H, Ar-H), 7.37–7.34 (m, 3H, Ar-H), 7.28–7.27(m, 3H, Ar-H), 7.10 (d, *J* = 8.0Hz, 2H, Ar-H), 6.68 (s, 2H, Ar-H), 5.46 (s, 2H, NCH₂), 3.73 (s, 2H, CH₂), 2.86(s, 6H, N(CH₃)₂). Minor isomer; δ 11.16 (s, 1H, OH), 7.72–6.68 (m, 15H, Ar-H), 5.22 (s, 2H, NCH₂), 3.73 (s, 2H, CH₂), 2.86 (s, 6H, N(CH₃)₂). HRESI-MS m/z calcd for [M+H]⁺: 439.21285, found: 439.21340.

4.2. Biology

4.2.1. Screening of cytotoxic activity

The methodology of the NCI anticancer screening has been described in detail elsewhere (<http://www.dtp.nci.nih.gov>), [39].

4.2.2. Cytotoxic activity using MTT Assay and evaluation of IC₅₀

4.2.2.1. MTT assay

MTT assay was performed to investigate the effect of the synthesized compounds on the viability of mammary epithelial cells (MCF-10A) [40, 41]. **See Appendix A.**

4.2.2.2. Assay for antiproliferative effect

To explore the antiproliferative potential of compounds MTT assay was performed according to previously reported procedure [42, 43] using different cell lines. **See Appendix A.**

4.2.2.3. Tubulin polymerization inhibitory activity

Tubulin assay was performed to evaluate the inhibitory potency of the most active compounds **IVc**, **IVf**, and **IVg** against tubulin [44, 45]. See **Appendix A**

4.2.2.4. EGFR inhibitory assay

EGFR-TK assay was performed to evaluate the inhibitory potency of the most active compounds **IVc**, **IVf**, and **IVg** against EGFR [46]. See **Appendix A**

4.2.2.5. BRAF kinase assay

V^{600E} mutant BRAF kinase assay was performed to investigate the activity of compounds **IVc**, **IVf**, and **IVg** against BRAF [47]. See **Appendix A**

4.2.2.6. Cell apoptosis assay

Apoptosis was determined by flow cytometry based on the Annexin-V-fluoresce in isothiocyanate (FITC) and propidium iodide (PI) staining kit (BD Pharmingen, San Diego, USA) [48, 49]. See **Appendix A**.

4.3. Molecular docking

The docking study was performed using the crystal structure of tubulin protein (PDB code: 5LYJ) [31] obtained from the Protein Data Bank (<https://www.rcsb.org/structure>). The study was performed by AutoDock 4.2 [32]. The ligands and protein files were prepared according to the previous reports [33, 34]. The grid and docking parameter files were prepared by AutoDock tools (ADT) following the previous reports [35, 36]. Visualization of the docking results and 2/3D binding modes of the new compounds were generated by Discovery Studio Visualizer [37] and by LigPlot⁺ (v.2.1) [38]. The results of the docking study were presented in **Table 6** and **Fig. 7-11**.

Acknowledgments

The authors acknowledge National Cancer Institute for the anticancer evaluation of the compounds on their 60-cell panel.

Conflicts of interest

The authors declare no conflict of interest

References

- [1] G.M. Alushin, G.C. Lander, E.H. Kellogg, R. Zhang, D. Baker, E. Nogales, High-resolution microtubule structures reveal the structural transitions in $\alpha\beta$ -tubulin upon GTP hydrolysis, *Cell*. 157 (2014) 1117–1129. doi: 10.1016/j.cell.2014.03.053.
- [2] H. Kadavath, R. V Hofele, J. Biernat, S. Kumar, K. Tepper, H. Urlaub, E. Mandelkow, M. Zweckstetter, Tau stabilizes microtubules by binding at the interface between tubulin heterodimers, *Proc. Natl. Acad. Sci.* 112 (2015) 7501–7506. doi:10.1073/pnas.1504081112.
- [3] A. Akhmanova, M.O. Steinmetz, Control of microtubule organization and dynamics: two ends in the limelight., *Nat. Rev. Mol. Cell Biol.* 16 (2015) 711–726. doi:10.1038/nrm4084.
- [4] A. Muroyama, T. Lechler, Microtubule organization, dynamics and functions in differentiated cells., *Development*. 144 (2017) 3012–3021. doi:10.1242/dev.153171.
- [5] C. Dumontet, M.A. Jordan, Microtubule-binding agents: a dynamic field of cancer therapeutics., *Nat. Rev. Drug Discov.* 9 (2010) 790–803. doi:10.1038/nrd3253.
- [6] G. Wang, F. Peng, D. Cao, Z. Yang, X. Han, J. Liu, W. Wu, L. He, L. Ma, J. Chen, Y. Sang, M. Xiang, A. Peng, Y. Wei, L. Chen, Design, synthesis and biological evaluation of millepachine derivatives as a new class of tubulin polymerization inhibitors, *Bioorg. Med. Chem.* 21 (2013) 6844–6854. doi: <https://doi.org/10.1016/j.bmc.2013.02.002>.

- [7] M.A. Jordan, K. Wendell, S. Gardiner, W.B. Derry, H. Copp, L. Wilson, Mitotic block induced in HeLa cells by low concentrations of paclitaxel (Taxol) results in abnormal mitotic exit and apoptotic cell death., *Cancer Res.* 56 (1996) 816–825.
- [8] I. Ojima, K. Kumar, D. Awasthi, J.G. Vineberg, Drug discovery targeting cell division proteins, microtubules and FtsZ., *Bioorg. Med. Chem.* 22 (2014) 5060–5077. doi: 10.1016/j.bmc.2014.02.036.
- [9] J. Xi, X. Zhu, Y. Feng, N. Huang, G. Luo, Y. Mao, X. Han, W. Tian, G. Wang, X. Han, R. Luo, Z. Huang, J. An, Development of a novel class of tubulin inhibitors with promising anticancer activities., *Mol. Cancer Res.* 11 (2013) 856–864. doi: 10.1158/1541-7786.MCR-12-0177.
- [10] R.B.G. Ravelli, B. Gigant, P.A. Curmi, I. Jourdain, S. Lachkar, A. Sobel, M. Knossow, Insight into tubulin regulation from a complex with colchicine and a stathmin-like domain, *Nature.* 428 (2004) 198-202. <http://dx.doi.org/10.1038/nature02393>.
- [11] B. Bhattacharyya, D. Panda, S. Gupta, M. Banerjee, Anti-mitotic activity of colchicine and the structural basis for its interaction with tubulin., *Med. Res. Rev.* 28 (2008) 155–183. doi:10.1002/med.20097.
- [12] L. Li, S. Jiang, X. Li, Y. Liu, J. Su, J. Chen, Recent advances in trimethoxyphenyl (TMP) based tubulin inhibitors targeting the colchicine binding site., *Eur. J. Med. Chem.* 151 (2018) 482–494. doi: 10.1016/j.ejmech.2018.04.011.
- [13] Y. Lu, J. Chen, M. Xiao, W. Li, D.D. Miller, An overview of tubulin inhibitors that interact with the colchicine binding site., *Pharm. Res.* 29 (2012) 2943–2971. doi:10.1007/s11095-012-0828-z.

- [14] A. Husain, A. Ahmad, A. Bhandari, V. Ram, Synthesis and antitubercular activity of pyridazinone derivatives, *J. Chil. Chem. Soc.* 56 (2011) 778–780. doi.org/10.4067/S0717-97072011000300013.
- [15] A. Husain, M.M. Alam, and N. Siddiqui, Synthesis, reactions and biological activity of 3-arylidene-5-(4-methylphenyl)-2(3H)-furanones. *J. Serb. Chem. Soc.* 74 (2009) 103-115. doi.org/10.2298/JSC0902103H
- [16] R. Bashir, S. Yaseen, S. Ovais, S. Ahmad, H. Hamid, M.S. Alam, M. Samim, K. Javed, Synthesis and biological evaluation of some novel sulfamoylphenyl-pyridazinone as anti-inflammatory agents (Part-II), *J. Enzyme Inhib. Med. Chem.* 27 (2012) 92–96. doi:10.3109/14756366.2011.577036.
- [17] K.A.M. Abouzid, N.A. Khalil, E.M. Ahmed, H.A.A. El-Latif, M.E. El-Araby, Structure-based molecular design, synthesis, and in vivo anti-inflammatory activity of pyridazinone derivatives as nonclassic COX-2 inhibitors, *Med. Chem. Res.* 19 (2010) 629–642. doi:10.1007/s00044-009-9218-4.
- [18] D. Kumar, R. Carron, C. De La Calle, D.P. Jindal, R. Bansal, Synthesis and evaluation of 2-substituted-6-phenyl-4,5-dihydropyridazin-3(2H)-ones as potent inodilators., *Acta Pharm.* 58 (2008) 393–405. doi:10.2478/v1007-008-0021-4.
- [19] A.A. Siddiqui, R. Mishra, M. Shaharyar, A. Husain, M. Rashid, P. Pal, Triazole incorporated pyridazinones as a new class of antihypertensive agents: design, synthesis, and in vivo screening., *Bioorg. Med. Chem. Lett.* 21 (2011) 1023–1026. doi:10.1016/j.bmcl.2010.12.028.

- [20] S. Ahmad, I.G. Rathish, S. Bano, M.S. Alam, K. Javed, Synthesis and biological evaluation of some novel 6-aryl-2-(p-sulfamylphenyl)-4,5-dihydropyridazin-3(2*H*)-ones as anti-cancer, antimicrobial, and anti-inflammatory agents., *J. Enzyme Inhib. Med. Chem.* 25 (2010) 266–271. doi:10.3109/14756360903155781.
- [21] S.H. Abbas, G.E.-D.A.A. Abuo-Rahma, M. Abdel-Aziz, O.M. Aly, E.A. Beshr, A.M. Gamal-Eldeen, Synthesis, cytotoxic activity, and tubulin polymerization inhibitory activity of new pyrrol-2(3*H*)-ones and pyridazin-3(2*H*)-ones, *Bioorg. Chem.* 66 (2016) 46–62. doi: <https://doi.org/10.1016/j.bioorg.2016.03.007>.
- [22] M.S. Abdelbaset, G.E.-D.A. Abuo-Rahma, M.H. Abdelrahman, M. Ramadan, B.G.M. Youssif, S.N.A. Bukhari, M.F.A. Mohamed, M. Abdel-Aziz, Novel pyrrol-2(3*H*)-ones and pyridazin-3(2*H*)-ones carrying quinoline scaffold as anti-proliferative tubulin polymerization inhibitors., *Bioorg. Chem.* 80 (2018) 151–163. doi: 10.1016/j.bioorg.2018.06.003.
- [23] J.K. Batra, L.J. Powers, F.D. Hess, E. Hamel, Derivatives of 5,6-diphenylpyridazin-3-one: synthetic antimitotic agents which interact with plant and mammalian tubulin at a new drug-binding site., *Cancer Res.* 46 (1986) 1889–1893.
- [24] M.F. El-shehry, K.M. Abu-zied, E.F. Ewies, S.M. Awad, M.E. Mohram, Synthesis of some novel azaheterocycles utilizing 3- (4-nitrobenzylidene) -5- phenylfuran-2(3*H*)-one with expected antimicrobial activity., *Der Pharma Chemica.* 5 (2013) 318–326.
- [25] M. Asif, Antifeedant, herbicidal and molluscicidal activities of pyridazinone compounds, *Mini. Rev. Org. Chem.* 10 (2013) 113–122. doi: [10.2174/1570193X11310020002](https://doi.org/10.2174/1570193X11310020002)
- [26] M. Böhm, I. Morano, B. Pieske, J.C. Rüegg, M. Wankerl, R. Zimmermann, E. Erdmann, Contribution of cAMP-phosphodiesterase inhibition and sensitization of the contractile proteins

for calcium to the inotropic effect of pimobendan in the failing human myocardium., *Circ. Res.* 68 (1991) 689–701. doi: 10.1161/01.res.68.3.689.

[27] M. Gökçe, Y. Dünder, E. Küpeİ, Synthesis of (6-Substituted-3 (2H)-pyridazinon-2-yl) acetic Acid and (6-Substituted-3 (2H)-pyridazinon-2-yl) acetamide Derivatives and Investigation of Their Analgesic and Anti-inflammatory Activities., *FABAD J. Pharm. Sci.* 35 (2010) 1-11.

[28] N.O. Mahmoodi, M. Jazayri, Direct synthesis of γ -butyrolactones via γ -phenyl substituted butric acids mediated benzyl radical cyclization., *Synth. Commun.* 31 (2001) 1467–1475. doi:10.1081/SCC-100104057.

[29] M.M. Alam, A. Husain, S.M. Hasan, Suruchi, T. Anwer, Synthesis and pharmacological evaluation of 2(3*H*)-furanones and 2(3*H*)-pyrrolones, combining analgesic and anti-inflammatory properties with reduced gastrointestinal toxicity and lipid peroxidation., *Eur. J. Med. Chem.* 44 (2009) 2636–2642. doi: 10.1016/j.ejmech.2008.10.030.

[30] C.S. Li, C. Brideau, C.C. Chan, C. Savoie, D. Claveau, S. Charleson, R. Gordon, G. Greig, J.Y. Gauthier, C.K. Lau, D. Riendeau, M. Thérien, E. Wong, P. Prasit, Pyridazinones as selective cyclooxygenase-2 inhibitors, *Bioorg. Med. Chem. Lett.* 13 (2003) 597–600. doi: [https://doi.org/10.1016/S0960-894X\(02\)01045-4](https://doi.org/10.1016/S0960-894X(02)01045-4).

[31] R. Gaspari, A.E. Prota, K. Bargsten, A. Cavalli, M.O. Steinmetz, Structural Basis of cis- and trans-Combretastatin Binding to Tubulin, *Chem.* 2 (2017) 102–113. doi: <https://doi.org/10.1016/j.chempr.2016.12.005>.

[32] G.M. Morris, R. Huey, W. Lindstrom, M.F. Sanner, R.K. Belew, D.S. Goodsell, A.J. Olson, AutoDock4 and AutoDockTools4: Automated docking with selective receptor flexibility, *J. Comput. Chem.* 30 (2009) 2785–2791. doi:10.1002/jcc.21256.

- [33] T.S. Ibrahim, R.M. Bokhtia, A.M.M. AL-Mahmoudy, E.S. Taher, M.A. AlAwadh, M. Elagawany, E.H. Abdel-Aal, S. Panda, A.M. Gouda, H.Z. Asfour, N.A. Alhakamy, B.G.M. Youssif, Design, synthesis and biological evaluation of novel 5-((substituted quinolin-3-yl/1-naphthyl) methylene)-3-substituted imidazolidin-2,4-dione as HIV-1 fusion inhibitors, *Bioorg. Chem.* 99 (2020) 103782. doi: <https://doi.org/10.1016/j.bioorg.2020.103782>.
- [34] M.S. Shaykoon, A.A. Marzouk, O.M. Soltan, A.S. Wanas, M.M. Radwan, A.M. Gouda, B.G.M. Youssif, M. Abdel-Aziz, Design, synthesis and antitrypanosomal activity of heteroaryl-based 1,2,4-triazole and 1,3,4-oxadiazole derivatives, *Bioorg. Chem.* 100 (2020) 103933. doi: <https://doi.org/10.1016/j.bioorg.2020.103933>.
- [35] A.M. Gouda, F.A. Almalki, Carprofen: a theoretical mechanistic study to investigate the impact of hydrophobic interactions of alkyl groups on modulation of COX - 1/2 binding selectivity, *SN Appl. Sci.* 1 (2019) 332. doi:10.1007/s42452-019-0335-5.
- [36] A.M. Shawky, M.A.S. Abourehab, A.N. Abdalla, A.M. Gouda, Optimization of pyrrolizine-based Schiff bases with 4-thiazolidinone motif: Design, synthesis and investigation of cytotoxicity and anti-inflammatory potency, *Eur. J. Med. Chem.* 185 (2020) 111780. doi: <https://doi.org/10.1016/j.ejmech.2019.111780>.
- [37] Dassault systems BIOVIA, Discovery Studio Visualizer, v16.1.0.15350, San Diego: Dassault systems, (2016).
- [38] R.A. Laskowski, M.B. Swindells, LigPlot+: multiple ligand-protein interaction diagrams for drug discovery., *J. Chem. Inf. Model.* 51 (2011) 2778–2786. doi:10.1021/ci200227u.
- [39] H.A.M. El-Sherief, B.G.M. Youssif, S.N.A. Bukhari, M. Abdel-Aziz, H.M. Abdel-Rahman, Novel 1,2,4-triazole derivatives as potential anticancer agents: Design, synthesis, molecular

docking, and mechanistic studies., *Bioorg. Chem.* 76 (2018) 314–325. doi: 10.1016/j.bioorg.2017.12.013.

[40] H.-L. Qin, J. Leng, B.G.M. Youssif, M.W. Amjad, M.A.G. Raja, M.A. Hussain, Z. Hussain, S.N. Kazmi, S.N.A. Bukhari, Synthesis, and mechanistic studies of curcumin analog-based oximes as potential anticancer agents., *Chem. Biol. Drug Des.* 90 (2017) 443–449. doi:10.1111/cbdd.12964.

[41] B.G.M. Youssif, M.H. Abdelrahman, A.H. Abdelazeem, M.A. Abdelgawad, H.M. Ibrahim, O.I.A. Salem, M.F.A. Mohamed, L. Treambleau, S.N.A. Bukhari, Design, synthesis, mechanistic and histopathological studies of small-molecules of novel indole-2-carboxamides and pyrazino[1,2-a]indol-1(2*H*)-ones as potential anticancer agents effecting the reactive oxygen species production., *Eur. J. Med. Chem.* 146 (2018) 260–273. doi: 10.1016/j.ejmech.2018.01.042.

[42] G.-F. Zha, H.-L. Qin, B.G.M. Youssif, M.W. Amjad, M.A.G. Raja, A.H. Abdelazeem, S.N.A. Bukhari, Discovery of potential anticancer multi-targeted ligustrazine based cyclohexanone and oxime analogs overcoming the cancer multidrug resistance., *Eur. J. Med. Chem.* 135 (2017) 34–48. doi: 10.1016/j.ejmech.2017.04.025.

[43] M. H. Abdelrahman, A. S. Aboraia, B. G. M. Youssif, B. E. M. Elsadek, Design, Synthesis and Pharmacophoric Model Building of New 3-Alkoxymethyl / 3-Phenyl indole-2-carboxamides with Potential Antiproliferative Activity, *Chem Biol Drug Des.* 90 (2017) 64-82.

[44] H.A.M. El-Sherief, B.G.M. Youssif, S.N. [Abbas Bukhari], A.H. Abdelazeem, M. Abdel-Aziz, H.M. Abdel-Rahman, Synthesis, anticancer activity and molecular modeling studies of

1,2,4-triazole derivatives as EGFR inhibitors, *Eur. J. Med. Chem.* 156 (2018) 774–789. doi: <https://doi.org/10.1016/j.ejmech.2018.07.024>.

[45] A.H. Abdelazeem, M.T. El-saadi, E.G. Said, B.G.M. Youssif, H.A. Omar, S.M. El-moghazy, *Bioorganic Chemistry Novel diphenylthiazole derivatives with multi-target mechanism: Synthesis, docking study, anticancer and anti-inflammatory activities*, *Bioorg. Chem.* 75 (2017) 127–138. doi: 10.1016/j.bioorg.2017.09.009.

[46] M. Hisham, B.G.M. Youssif, E.E.A. Osman, A.M. Hayallah, M. Abdel-Aziz, *Synthesis, and biological evaluation of novel xanthine derivatives as potential apoptotic antitumor agents.*, *Eur. J. Med. Chem.* 176 (2019) 117–128. doi: 10.1016/j.ejmech.2019.05.015.

[47] H.A.M. El-Sherief, B.G.M. Youssif, A.H. Abdelazeem, M. Abdel-Aziz, H.M. Abdel-Rahman, *Design, Synthesis and Antiproliferative Evaluation of Novel 1,2,4-Triazole/Schiff Base Hybrids with EGFR and B-RAF Inhibitory Activities.*, *Anticancer. Agents Med. Chem.* 19 (2019) 697–706. doi:10.2174/1871520619666181224115346.

[48] B.G.M. Youssif, A.M. Mohamed, E.E.A. Osman, O.F. Abou-Ghadir, D.H. Elnaggar, M.H. Abdelrahman, L. Treamblu, H.A.M. Gomaa, *5-Chlorobenzofuran-2-carboxamides: From allosteric CB1 modulators to potential apoptotic antitumor agents*, *Eur. J. Med. Chem.* 177 (2019) 1–11. doi: <https://doi.org/10.1016/j.ejmech.2019.05.040>.

[49] H.A. Abou-Zied, B.G.M. Youssif, M.F.A. Mohamed, A.M. Hayallah, M. Abdel-Aziz, *EGFR inhibitors and apoptotic inducers: Design, synthesis, anticancer activity, and docking studies of novel xanthine derivatives carrying chalcone moiety as hybrid molecules*, *Bioorg. Chem.* 89 (2019) 102997. doi: <https://doi.org/10.1016/j.bioorg.2019.102997>.

Highlights

- A novel series of Pyrrol-2-one, Pyridazin-3(2H)-one derivatives has been synthesized and tested by NCI for their anticancer activity.
- The **IVc** and **IVg** compounds showed excellent activity and were further selected for a five-dose assay.
- *In vitro* antiproliferative activity of compounds **IVc**, **IVf**, and **IVg** was evaluated using MTT assay.
- Compounds **IVc**, **IVf**, and **IVg** have been evaluated against EGFR, BRAF^{V600E} and Tubulin anticancer targets.
- A docking study of compounds **IVc**, **IVf** and **IVg** showed a strong fitting to the CA-4 binding sites in tubulin.

Graphical Abstract

